RESEARCH ARTICLE

Investigation of the temporal variability of thunderstorms in central and western Europe and the relation to large-scale flow and teleconnection patterns

David A. Piper[1] | Michael Kunz[1,2] | John T. Allen[3] | Susanna Mohr[1,2]

[1]Institute of Meteorology and Climate Research (IMK), Karlsruhe Institute of Technology (KIT), Karlsruhe, Germany

[2]Center for Disaster Management and Risk Reduction Technology, Karlsruhe Institute of Technology (KIT), Karlsruhe, Germany

[3]Department of Earth and Atmospheric Sciences, Central Michigan University, Mount Pleasant, Michigan, USA

Correspondence
Michael Kunz, Institute of Meteorology and Climate Research, Karlsruhe Institute of Technology (KIT), Hermann-von-Helmholtz-Platz 1, 76344 Eggenstein–Leopoldshafen, Karlsruhe, Germany.
Email: michael.kunz@kit.edu

Abstract

The driving factors that influence the spatial and annual variability of thunderstorms across Europe are still poorly understood. Due to a lack of long-term, reliable and consistent information about the occurrence of convective storms, a weather type classification has been developed that estimates thunderstorm probability from a combination of appropriate meteorological quantities on the mesoscale. Based on this approach, the temporal and spatial variability of convection-favouring environments is investigated between 1958 and 2014 using a high-resolution reanalysis dataset. To identify potential drivers for convective days, typical upper-level flow patterns were deduced using a multivariate approach. Our results suggest a strong link between local-scale thunderstorm activity and large-scale flow and air mass properties, such as stability, moisture, or vertical lifting. For example, while all over central Europe the most prominent pattern is given by a southwesterly flow type over the respective area, distinct regional discrepancies regarding further favourable flow types are observed. The crucial role of large-scale flow is further studied by assessing the relation between Northern Hemisphere teleconnection patterns and widespread convective activity. It is found that positive phases of the East Atlantic or Scandinavian patterns go along with a significant enhancement of convection-favouring conditions in several European regions, which can be explained by anomalies in the large-scale temperature and flow fields. Sea-surface temperature over the Bay of Biscay likewise impacts the convective environment, with the largest positive effect over the western part of the study area.

KEYWORDS

East Atlantic pattern, large-scale flow, NAO, North Atlantic Oscillation, SCAND, Scandinavian pattern, teleconnection patterns, thunderstorms, weather classification schemes

1 | INTRODUCTION

The drivers of the spatio-temporal variability in thunderstorm occurrence over Europe are poorly understood. Complicating understanding this problem further is that observational records that describe the underlying frequency of thunderstorms are incomplete, making such an analysis challenging (e.g. Groenemeijer *et al.*, 2017; Martius *et al.*, 2018). This issue is further exacerbated by the lack of a multinational observational dataset to provide a climate quality record for this type of analysis (Tippett *et al.*, 2015). To counteract these observational limitations, environmental proxies have commonly been applied to estimate the underlying convective frequency, leveraging conditions favourable to the development of thunderstorms (e.g. Brooks *et al.*, 2003; Brooks, 2009; Allen and Karoly, 2014; Mohr *et al.*, 2015a; Westermayer *et al.*, 2017; Taszarek *et al.*, 2019). While this approach is an effective methodology to estimate the underlying frequency of these events, it provides an incomplete picture, as not every environment favourable for the development of a thunderstorm ends up producing one (Brooks *et al.*, 2003). A number of approaches have attempted to remedy this issue including using model-derived convective precipitation (e.g. Allen *et al.*, 2015a; Groenemeijer *et al.*, 2017; Madonna *et al.*, 2018), matching of favourable environmental conditions with satellite overshooting top incidence (e.g. Punge *et al.*, 2017) or focusing on forcing mechanisms that lead to the initiation of thunderstorms such as objective weather types or regimes (Bissolli and Dittmann, 2001; Bissolli *et al.*, 2007; Kapsch *et al.*, 2012; Mohr *et al.*, 2015b). Another way to address the limitation is to explicitly simulate convection by downscaling reanalysis or model data to an appropriate scale, which has been found to be effective for more reliably estimating the frequency of severe convection over the USA (e.g. Trapp *et al.*, 2011; Robinson *et al.*, 2013; Gensini and Mote, 2014; Hoogewind *et al.*, 2017) and precipitation over the USA and Europe (e.g. Kendon *et al.*, 2017; Rasmussen *et al.*, 2017). However, the computations associated with such direct simulations at scales of less than 4 km are extensive, which has precluded long-term climatologies of more than 20–30 years (e.g. Trapp *et al.*, 2011; Rasmussen *et al.*, 2017), and these approaches have been typically directed toward assessing the impacts of climate change rather than climate variability. Despite these efforts, little attention has been paid to seasonal or to sub-seasonal climate variability of convective weather over Europe (Tippett *et al.*, 2015).

Teleconnections between remote climate signals and thunderstorm frequency have become an area of increasing focus in recent years (Barrett and Gensini, 2013; Lee *et al.*, 2013; Thompson and Roundy, 2013; Allen *et al.*, 2015b; Tippett *et al.*, 2015; Dowdy, 2016; Gensini and Marinaro, 2016; Molina *et al.*, 2016; Cook *et al.*, 2017; Allen *et al.*, 2018; Baggett *et al.*, 2018; Gensini and Allen, 2018; Tippett, 2018;

Trapp and Hoogewind, 2018). These modulations to frequency can lead to extreme differences in thunderstorm frequency from year to year, a pattern that is evident in European severe thunderstorm frequency (e.g. Kunz *et al.*, 2009; Mohr *et al.*, 2015a; Madonna *et al.*, 2018; Nisi *et al.*, 2018; Rädler *et al.*, 2018; Taszarek *et al.*, 2019). The primary drivers for this type of relationship are related to remote sea-surface temperatures (SST), the generation of tropical convection and the resulting influences on atmospheric Rossby waves and synoptic features (Tippett *et al.*, 2015). This influence on synoptic features has a downstream role in both the juxtaposition of the mesoscale convective environment and the large-scale forcing mechanisms relevant for convection initiation.

The signals with the largest certainty of influencing severe weather both over the USA and globally are the El Niño–Southern Oscillation (ENSO) on the seasonal scale, and the Madden–Julian Oscillation (MJO) on periods of less than a month. ENSO primarily influences the atmospheric circulation in the boreal autumn and winter, with the generation of anomalous convection over the central Pacific over anomalously warm SST disrupting the equatorial Walker circulation, establishing a subtropical jet and exciting downstream Rossby waves over North America, influencing the frequency and tracks of extratropical cyclogenesis, and has been shown to influence convective activity during the winter and spring (Lee *et al.*, 2013; Allen *et al.*, 2015b; Cook *et al.*, 2017). Similarly, the equatorial bursts of convection associated with the MJO can propagate into the regions upstream of continents, exciting Rossby waves and promoting the enhancement and subsequent wave breaking of the North Pacific jet stream, while also contributing to the poleward transport of tropical moisture (Barrett and Gensini, 2013; Thompson and Roundy, 2013; Tippett, 2018).

However, Europe's displacement from the central Pacific and the typically weak nature of both ENSO and MJO during the boreal summer months, when convection is most common over Europe, suggest that its influence may be weak (Marzban and Schaefer, 2001; Shaman, 2014; Guimares Nobre *et al.*, 2017). While there have been a number of studies addressing this topic over the USA for severe convection (hail and tornadoes), and a few efforts elsewhere globally (Allen and Karoly, 2014; Pinto, 2015; Dowdy, 2016; Blamey *et al.*, 2017), there have been comparatively few ones considering the drivers of thunderstorm variability over Europe (e.g. Mohr *et al.*, 2019). Piper and Kunz (2017), hereinafter referred to as PK17, identified a connection between lightning activity and the North Atlantic Oscillation (NAO), which they attributed to variations in the large-scale forcing leading to the development of thunderstorms. However, given the short temporal duration of this analysis, there was difficulty in obtaining statistically robust connections, and in identifying the role of more limited or regional teleconnections that may contribute to overall variability.

To address these challenges, we present a new method to estimate the likelihood of thunderstorms based on a weather regime proxy that estimates convection-favouring and convection-inhibiting environments. This proxy was developed using an observational proxy for widespread thunderstorm occurrences in western and central Europe, based on lightning detections over a period of 14 years, and then transferred to reanalysis data over 57 years. Leveraging the new weather regime proxy, large-scale flow patterns favourable to thunderstorm development are identified from reanalysis via empirical orthogonal function analysis. These large-scale flow patterns are then compared to those induced by various climate teleconnections and SST anomalies to establish the relevant drivers of the spatio-temporal variability of convection over Europe.

The article is structured as follows. Section 2 describes the model and observations datasets and briefly introduces the relevant teleconnnection patterns. Section 3 outlines the approach of convective weather type classification and principal component analyses. The results obtained for the the convection-favouring flow patterns, the weather type proxies, and the impact of teleconnection patterns and SST on convective activity are discussed in section 4. The last section 5 summarizes the results and gives some conclusions.

2 | MODEL DATA AND OBSERVATIONS

Convective activity across central and western Europe and its relation to environmental conditions is investigated using four convective proxies: (a) two model-based weather type proxies as convection-favouring (WMILX) and convection-inhibiting (CDSSX) patterns derived from reanalysis between 1958 and 2014 (section 2.2), and (b) two observational proxies based on lightning detections between 2001 and 2014 quantifying thunderstorm days (TDs) and days with widespread thunderstorms (WTDs; section 2.1); while the former are used for direct comparison with telecommunication indices, the latter serve only to develop the convective weather types.

The investigation area is central and western Europe, including France, Belgium, the Netherlands, Luxembourg, Germany, Switzerland, Austria, and parts of neighbouring countries. Because convective storms are most common in Europe during the warm summer months (Anderson and Klugmann, 2014; Punge and Kunz, 2016), the analyses are restricted to the summer half-year from April to September.

2.1 | EUCLID lightning detection

Convective activity is estimated from counts of flashes using the ground-based low-frequency lightning detection system BLIDS (BLitz InformationsDienst Siemens) for the period 2001–2014, which is part of the European Cooperation for
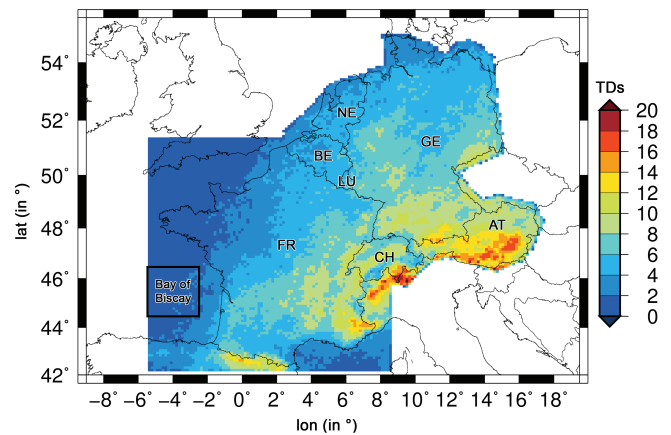
FIGURE 1 Mean annual number of thunderstorm days (TDs) during the summer half-year between 2001 and 2014 (adapted from PK17). The black box indicates the area over the Bay of Biscay where the SST was calculated (see section 2.4). AT, Austria; BE, Belgium; CH, Switzerland; FR, France; GE, Germany; LU, Luxembourg; NE, Netherlands; BE+NE+LU, Benelux

Lightning Detection (EUCLID) network. The detection efficiency of the system is around 96% for flashes with a peak current of at least 2 kA (Schulz *et al.*, 2016). Since the operational system implemented until 2015 had a significantly lower detection efficiency of cloud-to-cloud and intra-cloud lightning (Pohjola and Mäkelä, 2013), only cloud-to-ground flashes were used to assess the convective activity. Based on the technique of transit time, which builds upon the time shift of the electromagnetic wave detected at different sensors, the flashes can be located with an accuracy of around 100 m (Schulz *et al.*, 2016). Further information such as polarity or current strength are not considered.

As lightning density is dominated by single severe thunderstorm events producing several tens of thousands of flashes, we instead defined and considered the dichotomous variable *thunderstorm day* (TD). A day in our study is classified as TD when at least five flashes in 24 h are registered in a domain of the size of 10×10 km^2 (cf. Figure 1). PK17 have shown that this threshold represents an optimal value for the investigation area according to the empirical probability density distribution of daily flash numbers, which has an exponential shape (e.g. the probability P for 1 flash/24 h is 0.32, for two flashes is 0.13). Using the threshold of five flashes filters out 63.5% of all days with flashes. In addition, a given day is categorized as *widespread thunderstorm day* (WTD) if the number of flashes inside a specific sub-region exceeds its 75th percentile of the diurnal flash number. The calibration with respect to the 75th percentile is because the focus of our study is on strong and widespread thunderstorm activity rather than on isolated storms usually driven by local diabatically generated buoyancy.

TDs and WTDs are used for two purposes: to determine the convective weather types proxies of convection-favouring and convection-inhibiting patterns (section 3.1) and to

investigate the relationship between convective activity and predominant teleconnection patterns (section 4.3).

2.2 | Reanalysis

National Centers for Environmental Prediction/National Center for Atmospheric Research (NCEP/NCAR) R1 global reanalysis data (Kalnay *et al.*, 1996) are used to examine flow patterns and environmental conditions (dynamical/thermodynamical fields). The main advantages of this realization compared to the widely used NCEP/NCAR R2 (Kanamitsu *et al.*, 2002) are the extended availability from 1948 onward, and the data assimilation scheme that remained essentially unchanged during the project so that trends caused by temporal changes in the assimilated observations are minimized to a large degree. The investigation period is 1958–2014, excluding the relatively poor-quality data available prior to 1958. Data are available at 17 pressure levels with a spatial resolution of 2.5° × 2.5°. We considered wind vectors at 300 hPa, best representing planetary waves and the jet stream, respectively, and equivalent potential temperature θ_e at 850 hPa, where the direct influence of differential heating usually can be neglected. As convective activity peaks in the afternoon in most parts of the investigation area (Wapler, 2013; PK17), we used only the 1200 UTC data for a region spanning from 20°W to 30°E (30°W to 40°E) and from 35°N to 60°N (30°N to 60°N) for the flow patterns (anomalies of environmental conditions).

For computing the convective weather types, we additionally employed high-resolution coastDat-2 regional retrospective analysis (Geyer, 2014). This hindcast run was dynamically downscaled from NCEP/NCAR R1 using the Consortium for Small Scale Modelling (COSMO) model in climate mode (COSMO–CLM) Version 4.8 (Rockel *et al.*, 2008) with spectral nudging (Feser *et al.*, 2011). Thus, using these two reanalyses ensures consistency. CoastDat-2 runs are available from 1948 (including 3 years spin-up time) to 2014 in our archives. The temporal and horizontal resolution is 1 h and 0.22° (≈24 km), respectively, on 40 vertical model layers. Similar to the global reanalysis, 1200 UTC runs were used. For the purposes of this study, we considered a domain covering most of Europe and ranging from southern Spain in the southwest to Estonia in the northeast.

2.3 | Northern Hemisphere teleconnection patterns

To establish appropriate low-frequency modes of climate variability for analysis in relation to convective weather, teleconnections relevant for Europe during summer were considered. Focusing on the low-frequency modes yields several groups of regional, mutually correlated anomaly centres known as centres of action, which constitute dominant Northern Hemisphere Teleconnection Patterns (NHTPs). The variable strength of the centres of action and spatial shifts reflect natural climate variability.

Several studies have revealed that extreme precipitation and flooding in Europe vary in response to NAO, East Atlantic Pattern (EA), and Scandinavian Pattern (SCAND: e.g. Bueh and Nakamura, 2007; Casanueva Vicente *et al.*, 2014; Guimares Nobre *et al.*, 2017). In contrast, there is little apparent relationship between MJO and the summer months, and the weakened state of ENSO at this time of year means it reflects only a small contribution (Marzban and Schaefer, 2001; Guimares Nobre *et al.*, 2017). For that reason, we considered in our study only the NHTPs of NAO, EA and SCAND (note that we also investigated the East Atlantic Western Russian (EAWR) and Polar/Eurasian (POLEUR) Patterns which, however, showed no relation to convection).

Monthly time series of pattern amplitude of NAO, EA and SCAND between 1982 and 2014 were taken from the Climate Prediction Center of the US National Oceanic and Atmospheric Administration (NOAA). The NHTPs have been computed from NCEP-NCAR1 reanalysis using rotated S-mode principal component analysis (PCA: Richman, 1986), which isolates the primary patterns from monthly 500 hPa geopotential height anomaly between 20°N and 90°N (Barnston and Livezey, 1987). The indices are standardized by the 1981–2010 climatology, resulting in similar value ranges with (dimensionless) means and medians between 0 and 1, and 99th percentiles of ±3 (cf. Table 1).

NAO is the leading principle component of variability for many atmospheric phenomena during the summer (Folland *et al.*, 2009; Casanueva Vicente *et al.*, 2014; Guimares Nobre *et al.*, 2017), but is associated with a weakened anomaly compared to its stronger pattern during winter. More broadly, NAO is the strongest of all NHTPs, being the only pattern found for every month of the year. It is represented by a dipole of anomalies in north-to-south direction (Barnston and Livezey, 1987; Hurrell *et al.*, 2003), located over Greenland and the central latitudes between 35°N and 40°N of the North Atlantic. Negative phases of NAO reflect above-normal geopotential heights across high latitudes combined with below-normal heights over the central North Atlantic and have been shown to enhance precipitation and modulate the cyclonic track southwards (Folland *et al.*, 2009). Positive phases are expressed through a reverse arrangement that prevails in the same regions, and have been noted to be associated with reduced precipitation over the continent (Folland *et al.*, 2009; Casanueva Vicente *et al.*, 2014).

The EA, which also strongly contributes during all seasons, is the second major NHTP over the North Atlantic (Barnston and Livezey, 1987; Krichak and Alpert, 2005). Similar to the NAO, the EA expresses a north-to-south oriented dipole spanning the North Atlantic from east to west. Compared to the dipole associated with the NAO, the

TABLE 1 Range of values (mean, median and different percentiles) for the dimensionless NHTP indices of NAO, EA and SCAND (1958–2014)

	Mean	Med	1st	5th	95th	99th
NAO	−0.02	0.02	−2.38	−1.63	1.56	2.06
EA	−0.20	−0.16	−2.68	−1.89	1.40	1.83
SCAND	0.14	0.20	−2.09	−1.53	1.63	2.30

influence of the EA is slightly shifted to the southeast, with similar responses in precipitation (Casanueva Vicente *et al.*, 2014).

Finally, the SCAND pattern consists of a primary centre of geopotential anomaly over Scandinavia and weaker centres with opposite sign over western Europe and eastern Russia (Bueh and Nakamura, 2007). While negative phases are associated with negative height anomalies in these regions, positive phases reflect positive geopotential anomalies over Scandinavia and western Russia, sometimes associated with blocking events.

2.4 | Sea-surface temperature

In addition to the NHTPs, we also analysed upstream anomalies of SST representing a significant contribution to the natural variability of the climate system which can locally modulate the atmospheric circulation, particularly in terms of moisture availability (e.g. Piazza *et al.*, 2016; Miglietta *et al.*, 2017). In our study, we used the NOAA Optimum Interpolation (OI) SST V2, which is interpolated from direct and indirect measurements on a global grid with a spatial resolution of $1° \times 1°$ (Reynolds *et al.*, 2002). The analysis uses *in situ* and satellite observations plus SSTs simulated by sea-ice cover. For reasons of consistency with NHTPs, we used monthly means from 1982 to 2014 generated from daily fields. The monthly gridded data were averaged over the Bay of Biscay (cf. black box in Figure 1) in an area of the size $3° \times 2°$ between 44.5°N/5.5°W and 46.5°N/2.5°W. SST anomaly originally was computed by subtracting the long-term mean (for that location at that time of year) from the current monthly mean value at each grid point.

3 | METHODS

3.1 | Convective weather types

Convective activity shows considerable spatial differences as can be seen in Figure 1 for the mean number of TDs. For this reason, we have subdivided the whole investigation area into a total of 108 mesoscale sub-regions with a size of 15×15 grid points (approx. $3.1° \times 3.1°$), for which we estimated convective weather patterns and the relation to driving mechanisms. The individual sub-regions are separated from each other by 7 grid points in *x*- and *y*-directions. For each day the variables

defining the convective weather types are averaged over a certain sub-region.

To estimate convective activity over a period significantly longer than the lightning detections, a new convective weather type (CWT) classification scheme was developed using the coastDat-2 hindcast runs (section 2.2). This scheme is similar to the objective classification scheme of the German Weather Service (DWD), which maps four continuous meteorological variables (large-scale flow direction, cyclonicity at two levels, precipitable water related to the climatology) to binary variables (0/1), depending on whether a predefined threshold was exceeded or not, yielding 40 different weather types (Bissolli and Dittmann, 2001; Kapsch *et al.*, 2012). Based on categorical verification, however, this scheme proved to have very limited prediction skill for WTDs. The maximum Heidke Skill Score for specific convective weather types was HSS = 0.18; the Brier Skill Score using all weather types was only BSS = 0.20 (see appendix for a brief description of the skill scores). For this reason, we have replaced the original variables by variables that are related to convection considering both dynamic (uplift) and thermodynamic (thermal stability, moisture content) properties of the air masses. The main requirement of our new scheme is that it separates classes (days) with very high and low probability of widespread thunderstorms (WTD) very well from each other and from the continuum of possible multivariate states of the atmosphere. Similar to the DWD classification, the grid points defining a sub-region are weighted differently according to their distance from the centre: grid points in the centre of the domain are weighted three times, those at a distance of four grid points (0.88°) from the boundaries of the inner sub-region two times, and those at a distance between 5 and 8 by a factor of 1. A combination of at least one thermodynamic and one dynamic quantity is required to capture the conditions for widespread convection. In total we have tested 12 different variables (cf. Table 2) in various combinations of either three or four variables with varying thresholds. These variables have proved to be most suitable for hailstorm prediction in central Europe according to a logistic regression model in the study of Mohr *et al.* (2015b, see table A1).

Replacing the flow direction in the DWD scheme by the Surface Lifted Index (*SLI*; Galway, 1956) already leads to a significant improvement of the prediction skill (BSS increases from 0.20 to 0.33). Since the effect of cyclonicity (proportional to the relative vorticity) is physically related to

TABLE 2 Variables considered in the development of the CWT scheme. Those variables finally used in the scheme are in bold, those where an annual cycle is subtracted are in italic letters

Thermodynamical	Dynamical
Flow direction (700 hPa)	Relative vorticity (two levels)
Precipitable water	Vorticity advection (300 hPa)
Spec. humidity (950 hPa)	Horiz. divergence (300 hPa)
Dew-point (2 m; 0600 UTC)	Q-vector divergence (500 hPa)
Daily maximum temp. (2 m)	**Vertical lifting (500 hPa)**
Equiv. pot. temp. (850 hPa)	
Surface Lifted Index	

TABLE 3 Thresholds of the input parameters equivalent potential temperature in 850 hPa (θ_e), precipitable water (pw), Surface Lifted Index (SLI), and vertical wind speed (w) used for the CWT classification. While threshold 1 (th1) defines convection-favouring parameters, threshold 2 (th2) is for convection-inhibiting parameters

	θ_e	pw	SLI	w
th1	≥ 279.6 K	≥ 41.0 kg m^{-2}	≤ 0.09 K	≥ 0.07 m s^{-1}
th2	≤ 275.8 K	≤ 18.8 kg m^{-2}	≥ 1.88 K	≤ -0.01 m s^{-1}

vertical motion, we replaced one of these parameters by vertical velocity at 500 hPa, w_{500}, while the other one is replaced by equivalent potential temperature at 850 hPa ($\theta_{e\,850}$). These two replacements further increase BSS from 0.33 to 0.48. Precipitable water (pw) as an index for the moisture content was found to be important and remained unchanged. Thus, the final set of variables selected for the CWT classification is: $\theta_{e\,850}$, pw, SLI, w_{500}. For the former two variables, high-frequency variability is reduced by subtracting the 10-day running mean from the average daily values.

The continuous variables $\theta_{e\,850}$, pw, SLI, w_{500} are mapped to discrete and trichotomous ones (PT, PW, LI, VV) using an upper and lower threshold for each parameter determined by an objective method. The advantage of the trichotomous compared to the widely used dichotomous scheme is that values that differ only slightly but are located between the lower and upper thresholds the threshold (e.g. $SLI = 0.1$ and 0.08 K; threshold = 0.09 K; cf. Table 3), do not change to the opposite class (here: from stable to unstable), but to a neutral class. In order to determine the threshold that distinguish best between environments favouring (threshold 1) or inhibiting convection (threshold 2), we calculated the distribution of the obtained HSS with respect to WTDs on a large range of possible threshold values for each parameter. The two values, where HSS equals its 90th percentile, are then considered as the two thresholds (Table 3); values between are assigned to the neutral class (denoted as X). The CWT classification scheme yields in total $3^4 = 81$ classes in the arrangement of PT PW LI VV.

Categorical verification (Wilks, 2011) is also used to assess the prediction skill of the 81 weather types. When developing and evaluating the CWT classification scheme, we have not distinguished between a training and a verification period. Since lightning detections were available only for 14 years, a subdivision of the data, for example into two 7-year periods, would have resulted in too short periods of time. According to the results shown in Figure 2, the two patterns characterized by warm (PT = W) and moist (PW = M) air masses, prevailing latent instability (LI = I) and either synoptic-scale lifting (VV = L) or no vertical motion (X) present, aggregated by WMILX (combination of WMIL and WMIX), yield the highest HSS of 0.27 for the prediction of WTDs. This comparatively low value is primarily due to a low probability of detection (POD) of only about 22% for WTDs (not shown). On the other hand, the false alarm rate (FAR) is extremely low with just 6.5%. This means that the probability of widespread thunderstorms on a WMILX day is 93.5%. Conversely, scattered thunderstorms may also develop on days classified with a different parameter combination. This result confirms our goal to create a proxy with a very high probability of widespread thunderstorms. The opposing situation with cold (PT = C), dry (PW = D), stable (LI = S) conditions with either subsidence (VV = S) or no vertical motion (X) is captured by the two patterns CDSS and CDSX, which are combined to the single pattern CDSSX. The HSS for this proxy is 0.38 (note that the negative sign in Figure 2 is due to the WTD proxy used for the evaluation) with an FAR of only about 3%. Thus, thunderstorms are extremely rare on days classified as CDSSX, even if days without thunderstorms may also be captured by other parameter combinations.

Averaged over the entire study area and the 57-year period, the CWT classification quantifies a significantly lower number of convection-favouring WMILX days (8.1 ± 5.4 days/half-year, corresponding to $4.4 \pm 2.9\%$ of all days from April to September) compared to convection-inhibiting CDSSX days (65.3 ± 17.5 days/half-year, $35.7 \pm 9.6\%$), reconfirming how strict this classification is for convective days. For this reason and the fact that the other 77 types exhibit only a low prediction skill for convection (cf. Figure 2), the following investigations refer to these two weather pattern proxies only.

3.2 | T-mode PCA

Based on the above-defined WMILX days, we apply a rotated T-mode PCA to the 1200 UTC geopotential fields at 500 hPa to determine characteristic convection-favouring flow patterns (Huth, 1996). This is equivalent to rotating the basis vectors such that the first one points in the direction of maximum variance, the second one in the direction of maximum residual variance, and so on. Hence, the input data are projected onto a new orthogonal basis (e.g. von Storch and Zwiers, 2001). Due to the principle of variance maximization,
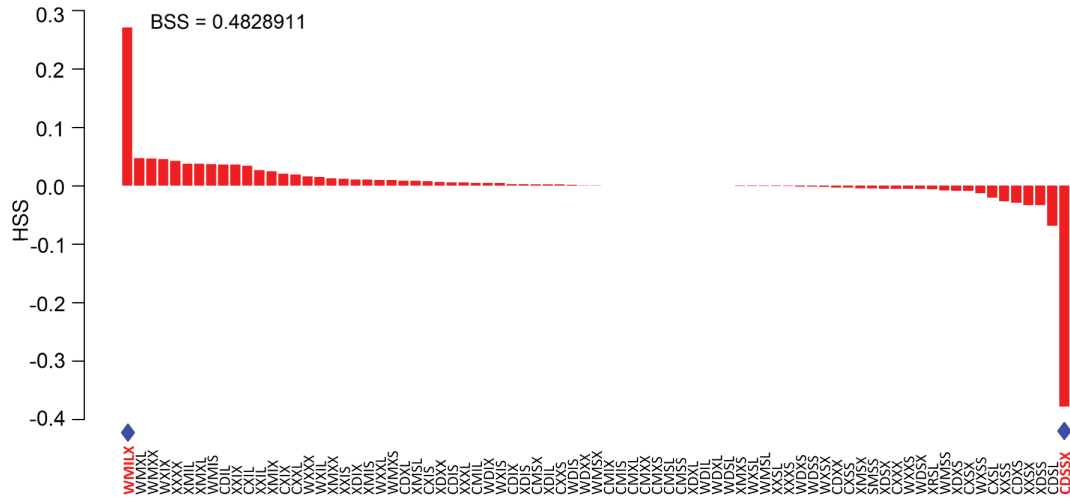
FIGURE 2 Evaluation of the prediction skill using the Heidke skill score HSS of the CWT classification for days characterized as widespread thunderstorm days (WTDs) according to lightning detections (2001–2014). The two proxies WMILX and CDSSX indicated received by far the highest HSS values

the sample of input fields can be reduced to a small set of output fields, represented by the leading principle components (PCs). Following Richman (1986), we rotated the PCs and loading vectors in the form of a linear transformation to generate characteristic fields, which are a measure of each of the principal factors used. The loading vector describes the relevance of the characteristics to the PCs (coefficients) and expresses the strength and orientation of the relationship between the characteristics (influence variables) and the factors. If the loading is small for all PCs, the characteristic has minor relevance for the description of the objects (Philipp, 2009). As suggested by Huth (2000), we used an oblique rotation algorithm instead of an orthogonal one.

Different criteria are available to determine the number of PCs to be retained for rotation. We apply the approach discussed in North *et al.* (1982) and O'Lenic and Livezey (1988), which is to cut the number of PCs behind pairs of close eigenvalues. For this purpose, the eigenvalue is plotted over the order number (scree plot); then the position is searched where two adjacent values form a kind of plateau after the initial steep drop (e.g. Huth, 1996). If this criterion yields more than one possibility, the respective PC sets are carefully checked for their ability to reproduce the input fields. For this purpose, we determine in each case the average value of the maximum loading in relation to the individual input fields, and the average difference between the two highest loadings.

3.3 | Impact of teleconnections on convective activity

The impact of NHTPs on thunderstorm activity is investigated using two convective proxies: TDs quantified from lightning over a 14-year period (cf. section 2.1) and WMILX/CDSSX based on costDat-2 reanalysis for a 57-year period (cf. section 2.2). Rather than relying on absolute values, we calculated

relative deviations of the frequency of the two convective proxies from the climatology during specific phases of NHTP patterns for each grid point/sub-region. The relative deviation D measuring the influence of the NHTP indices on convective activity is expressed by:

$$D = \frac{\hat{p}\{a = 1 \mid \text{NHTP} \gtrless \pm X\}}{\hat{p}\{a = 1\}} - 1, \tag{1}$$

where $\hat{p}\{a|b\}$ denotes the conditional probability of event a (TD or CWT/WMILX) given event b (=NHTP). Since our focus is on significantly negative/positive phases of the teleconnection patterns, Equation 1 considered a threshold X for the index values, which is ±0.5 in the case of EA and ±1.0 for SCAND and NAO. The analysis was conducted over the entire half-year rather than over individual months, as the NHTPs are not subject to strong spatial shifts in summer. A value of $D = 1$ signifies a doubling of the relative frequency of the respective convective proxy during the respective phase (positive or negative) as compared to the total sample. Likewise, $D = -1$ implies complete suppression of TDs or WMILX/CDSSX patterns. Statistical significance is assessed using a two-sided bootstrap test (α in {.05, .10}) based on the test statistic D with the null hypothesis H_0 stating that a given non-zero value of D is simply due to chance.

4 | RESULTS

Using data for the entire coastDat-2 hindcast run (1958–2014; April–September), the following section examines characteristic convection-favouring flow fields (section 4.1), the spatial distribution of convective environments with regard to the newly developed CWT proxy of convection-favouring (WMILX) and convection-inhibiting (CDSSX) patterns (section 4.2), and the relation between TDs/CWT proxies
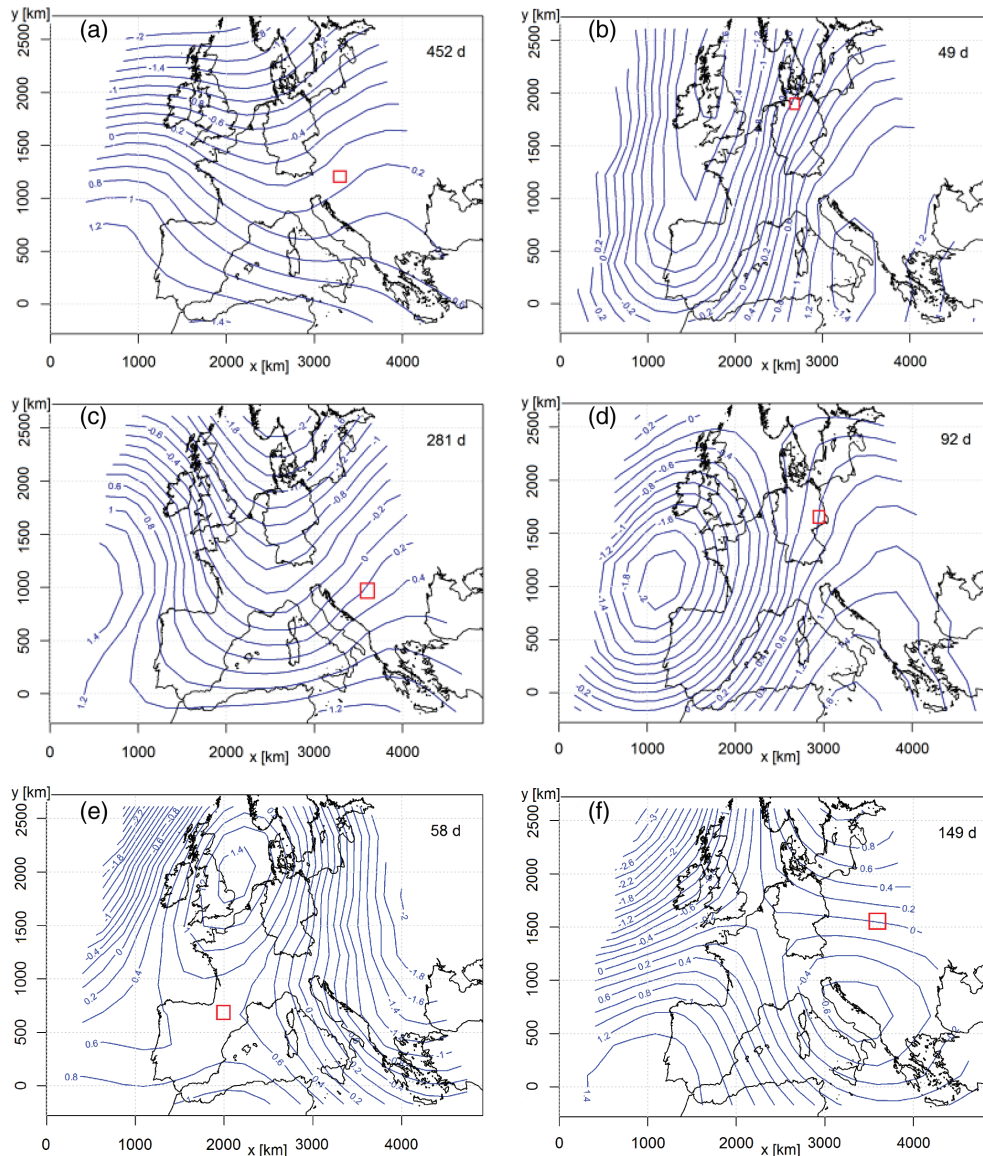
FIGURE 3 (a–f) Examples of flow configurations associated with convection-favouring conditions (WMILX) within different reference areas (red squares). Indicated (top right) in each subfigure is the number of days [d] that prevailed for that configuration during the period 1958–2014

and teleconnection indices and SST, including anomalies of geopotential and temperature distributions (section 4.3).

4.1 | Characteristic convection-favouring flow patterns

Characteristic flow patterns that prevail on average on WMILX days are examined by applying a T-mode PCA on the 1200 UTC geopotential fields at 500 hPa. According to the assessment of the scree plot as proposed by North *et al.* (1982) and optimizing the average maximum loading, we obtained an optimum number of four rotated PCs for all mesoscale sub-regions. The PCs shown in Figures 3 are dimensionless, but are equivalent to the geopotential field. Most of the WMILX days in the respective sub-regions are dominated by a southerly to southwesterly upper-level flow as observed

in other studies concerning thunderstorm or hail events in Europe (e.g. Kapsch *et al.*, 2012; Merino *et al.*, 2014; Wapler and James, 2015; Nisi *et al.*, 2016; Mohr *et al.*, 2019).

Figure 3 illustrates the manifold forms of these southwesterly flow patterns for four exemplary sub-regions (indicated by the red box). For southeastern Austria, for example, the geopotential field is characterized by a short-wave and low-amplitude trough with its axis spanning over western Germany (Figure 3a). In contrast, the sub-region in northern Germany shows a deep trough extending far southward with its axis over the British Isles, which leads to a nearly southerly upper-level flow (Figure 3b). The two patterns for Bosnia and Saxony in eastern Germany (Figure 3c,d) exhibit an intermediate degree of meridional flow, but with different geopotential gradients and relative distances to the trough axis. The geopotential patterns shown in Figure 3 suggest

a trough to be present upstream of the sub-regions, which allows for both the advection of warm and moist air masses and large-scale lifting due to positive vorticity advection. Moreover, embedded short-wave troughs usually associated with intense quasi-geostrophic ascent additionally facilitate convection initiation.

However, flow patterns distinctly different from the southwesterly types may also provide environments conductive to the development of widespread convection. Along the southern Pyrenees, for instance, such conditions occur preferably when a closed upper-level ridge is located to the south (Figure 3e). In this case, convection inhibition due to subsidence primarily takes place ahead of the closed high. Over the southern Pyrenees, unstable air masses are frequently advected by the low-level wind field along topographically favoured channels, for example via the Ebro valley. Over southern Poland (Figure 3f), convection often evolve in combination with an easterly or southeasterly flow between a closed upper-level low associated with the advection of warm and moist air from the Black Sea in combination with large-scale lifting north of the trough. This pattern provides evidence of another important pathway for convection-favouring air masses being advected to central Europe aside from the dominant southwesterly flow. In addition, it highlights the role of the barrier formed by the Alpine ranges, leading to convection-favouring conditions for both southwesterly and easterly–southeasterly advection pathways.

4.2 | Climatology of convective environments

The frequency of the two CWT proxies shows considerable differences over the entire study area. The highest number of days with convection-favouring patterns (WMILX) prevails in an arched–curved swath extending from the Pyrenees in the west over southern Germany to Slovakia in the east (average 15–17 days per year; Figure 4a). In the northwest, the number of WMILX days substantially decrease to less than 5. Over the Bay of Biscay or the Baltic Sea, only 2–3 WMILX days per year prevail. West of Cornwall and over parts of the North Sea, such days do not occur at all, mainly reflecting the influence of the ocean on atmospheric stability (Mohr and Kunz, 2013). Overall, a positive gradient in WMILX frequency is identified both in north-to-west and west-to-east directions, that is, along the coastlines of the North Atlantic and the Baltic Sea. This general distribution of convective environments is confirmed by similar studies based on reanalysis (Mohr *et al.*, 2015a; Prein and Holland, 2018; Rädler *et al.*, 2018; Taszarek *et al.*, 2019), lightning (PK17; Taszarek *et al.*, 2019), and satellite (Punge *et al.*, 2017) data. However, there are major differences in the area of the Alps and their surroundings, mainly because orographically induced circulations and
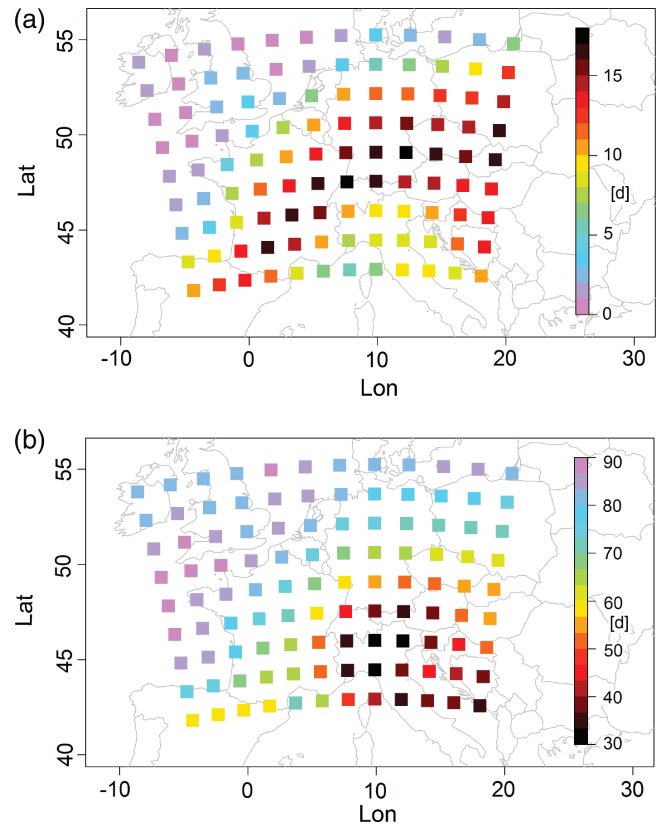
FIGURE 4 Mean annual frequency of days [d] with (a) convection-favouring (WMILX) and (b) convection-inhibiting (CDSSX) environment conditions prevailing in the sub-regions of size 3.1° × 3.1° according to the CWT approach applied to coastDat-2 hindcast between 1958 and 2014 (note that for reasons of better visibility the sub-regions are displayed in smaller sizes)

resulting convergence zones, which are mainly relevant for the triggering of convection, are not sufficiently resolved by the coastDat-2 reanalysis.

The distribution of thunderstorm-inhibiting CDSSX days is almost reversed compared to that of WMILX days (Figure 4b; note the reverse colour sequence). In most regions, an increased number of WMILX days goes along with a reduced number of CDSSX days and vice versa. For example, over the Atlantic, North Sea and Baltic Sea, up to 90 CDSSX days prevail on average, while about only half prevail in regions with high convective activity such as southern Germany. Only in northern Italy can a marked difference be observed, where CDSSX days have a minimum of about 30 days.

The spatial distributions of WMILX and CDSSX days suggest the flow patterns to be the general driver as discussed in the previous section. Northward advection of unstable stratified subtropical air masses at the western foothills of the Alps is assumed to cause the increased thunderstorm frequency in central France and southern Germany. In addition, the elevated frequency of WMILX days over the eastern parts of the study area confirms the second dominant advection path of convection-favouring air masses from the Black Sea,

north-eastern Mediterranean and Adriatic Sea as discussed in section 4.1.

The comparatively low frequency of convection-favouring WMILX days over northern Italy, where the observed probability of thunderstorms is very high (Feudale and Manzato, 2014; Nisi *et al.*, 2016), follows from the classification scheme based on anomalies of θ_e and *pw* rather than on absolute values. Compared to other regions with lower mean values, threshold exceedance occurs less frequently here, so that thunderstorm-favouring conditions prevail even for neutral values of these two parameters. Note that the *SLI*, which takes absolute values into account in the CWT scheme, has an absolute minimum (i.e. maximum of potential instability) in northern Italy (not shown). This results in a lower number of days with reduced convection in that region due to the high frequency of days with increased instability. In combination with the distribution of comparably few WMILX days, this suggests that instability conditions are often met, but large-scale forcing is more limited, thereby reducing the probability of widespread convection, as also found, for example, by ?. Another reason for the low number of WMILX days here is that the scheme is not able to consider all convection triggering mechanisms, especially those related to local-scale lifting associated with flow deviations at mountains.

The time series of the annual number of days with both convection-favouring WMILX and convection-inhibiting CDSSX weather types (Figure 5) averaged over the sub-regions of Germany as an example show a large annual and multi-annual variability. The frequency of WMILX days ranges between 3 and 22, that is, between 1.6 and 12.6% (average: 9.8 days or 5.4%) related to all days of the summer half-year. Conversely, days with convection-inhibiting conditions fluctuate between 52 and 95 days (28.4–51.9%; average: 73.9 days or 40.4%). The remaining days (55.2%) are either related to other CWT patterns or to neutral values for one of the parameters PT, PW or LI, and thus discarded from the analysis.

Overall, the two time series show no significant trends when looking at the entire 57-year period (cf. Mohr *et al.*, 2015a). Only when the series of WMILX is split around the mid-1980s can a positive trend for the second part be analysed, which is mainly due to (statistically significant) increasing values of θ_e, while simultaneously large-scale lifting *w* decreased (also *pw* and *SLI* have trends towards convection-favouring conditions, but with a lack of statistical significance; cf. Piper, 2017). This increase of convection-favouring conditions for thunderstorm or hail development since the 1980s has been already observed by other studies (Kapsch *et al.*, 2012; Mohr and Kunz, 2013; Rädler *et al.*, 2018).

The power spectrum of WMILX days obtained by application of a Fast Fourier Transform (FFT) show distinct peaks at longer periods of 5.4, 9.2 and 12.8 years (not shown). For
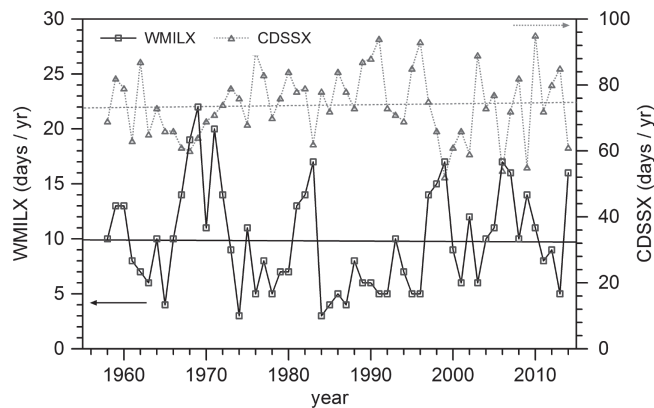
FIGURE 5 Time series of convection-favouring (WMILX; solid black line) and convection-inhibiting (CDSSX; dashed grey line) environment conditions prevailing over the sub-regions of Germany including linear trends for the whole period

CDSSX days the strongest peak occurs at 2.4 years, but power density is also slightly enhanced between 5 and 8 years. Even though the two time series substantially differ concerning the magnitude of the fluctuations and the dominant frequencies, both are dominated by multi-annual fluctuations. Apart from random fluctuations inherent in the dynamic and thermodynamic variables that define the CWT proxies, the peaks at longer periods imply large-scale atmospheric patterns such as teleconnections act as an important mechanism for convective activity, which will be investigated in the next section.

4.3 | Relation between teleconnection patterns and convective activity

The large-scale geopotential fields discussed above are subject to the superposition of differing temporal variability modes of the climate system (Wallace and Gutzler, 1981; Barnston and Livezey, 1987). The low-frequency modes are represented by dominant NHTPs, with variable strengths and spatial shifts of their centres of action reflecting natural climate variability.

In the following, we evaluate and assess relationships between the most important NHTPs (NAO, EA, SCAND) and convective activity by considering two proxies: TDs determined from lightning data (14-year period; section 2.1) and convection-favouring WMILX days from the CWT classification (33-year period, as data for the NHTPs have only been available since 1982; section 3.1). Recall that, in addition to the time periods, also the characteristics of convective activity differ between the two proxies: while TDs refer to small areas of the size 10×10 km^2 and thus also capture local convection, WMILX days are trained for widespread convection in the respective sub-regions (cf. section 3.1).

4.3.1 | North Atlantic Oscillation

The NAO is one of the most important modes of variability in the atmospheric circulation for Europe, both in the winter

and summer (Folland *et al.*, 2009), though somewhat weaker in the summer. NAO has been shown by PK17 to have a strong influence on convective activity across Europe. Also, in northern Italy, a significant relationship is found between the number of hail days in the warm season and the NAO index of the following winter (Giaiotti *et al.*, 2003). For the sake of completeness, we give here a brief summary of the main findings of PK17 with regard to NAO variability in the context of the present study.

Over most parts of the study area, the TD frequency was found to be considerably increased during negative NAO phases (NAO_-) and decreased for positive phases (NAO_+; see Fig. 12 in PK17). The increases in former cases were particularly strong in (eastern) Austria, southern Germany, and eastern France (except the French Maritime Alps), whereas the strongest decreases during NAO_+ occurred over parts of northern Germany, northeast Austria, and in an area extending from southwestern Switzerland to the Mediterranean. Statistical significance of the relationship, however, was confined to only about 20% of the total area for both phases. The low statistical significance for TDs is mainly due to the large temporal variability, the short observation period and, above all, the fact that the TD sample is also contaminated by scattered, unorganized convective cells. Related triggering mechanisms such as low-level flow convergence are certainly not related to NHTPs. As we will see in the following, the low statistical significance applies to the relationship between all NHTPs and TDs.

Unlike TDs, the CWT proxy WMILX shows only minor variations in response to different NAO phases. During NAO_- patterns, WMILX days are slightly above average for most of the sub-regions. Likewise for NAO_+, several sub-regions showed an increased probability for thunderstorms, but also with limited significance for most sub-regions (see Fig. 8.15 in Piper, 2017).

The initially surprising discrepancy between reduced TDs and increased WMILX days during NAO_+ can be explained by the different types of convection inherent in the two proxies as already alluded to above. Another explanation is the special configuration of the jet stream during this phase. The relocation of the associated frontal zone to Scandinavia implies a predominance of strong and extended ridges over central Europe associated with a lack of required lifting forcing. However, if all three thermodynamic parameters in the CWT classification scheme (PT, PW, LI) indicated convection-favouring parameters, a neutral value of the lifting parameter VV is sufficient to classify a day as a WMILX day.

4.3.2 | East Atlantic Pattern

The second leading mode of variability in Europe is the East Atlantic Pattern (EA), which is known, for example, for its influence on precipitation intensity in the Mediterranean region (Krichak and Alpert, 2005). The analysis of lightning data shows that EA has a significant and regionally variable influence on convective activity at several locations (Figure 6). Negative phases ($EA_- < -0.5$) are associated with markedly reduced TD frequencies (negative D; cf. Equation 1) over large parts of the investigation area, with the exception of the west and south of France (Figure 6a). A salient feature is the almost contiguous zone with a negative, mostly significant signal ($D < -0.7$) covering large parts of the southern Alpine region of Switzerland and Austria. In contrast, convective activity is found to be slightly increased, albeit not significantly, on the Mediterranean coastline of the southeast corner of France. Although statistical significance is very patchy, a significance of at least $Si = 90\%$ is achieved at around 21% of all grid cells (Figure 6b). However, when considering only the area east of $x = 1,000$ km and north of $y = 400$ km (approx. 45.5°N, 6°E) including Germany, Switzerland, Austria, and the eastern part of France, the number of significant grid points increases to 54%. In Austria even 80.8% of all grid points show a significant relation. During positive phases ($EA_+ > 0.5$; Figure 6c,d), TD frequency increases nearly ubiquitously across the domain, except of the lower Rhône valley, where the number is slightly reduced. However, almost all grid points (<3%) lack statistical significance.

Anomalies in the monthly frequency of WMILX days according to the CWT classification yield an even more robust separation of convective activity. Negative EA_- phases are predominantly characterized by a reduced probability of WMILX days, statistically significant in a broad stripe between the Benelux Union and the Balkan Peninsula in southeastern Europe (Figure 7a,b). In contrast during EA_+ phases, an increase in WMILX days can be observed in most of the sub-regions (Figure 6c) similar to the results of the TDs. This increase is significant over large parts of Germany and adjacent regions (Figure 7c,d). For both EA phases, the magnitude of the change signal D for WMILX days is similar to that of TDs.

Exploring the large-scale fields, EA_- corresponds to a positive geopotential anomaly west of the British Isles coupled with a negative centre stretching from northwestern Africa to eastern Europe (Figure 8). This configuration leads to a northerly to northwesterly upper-level flow over central Europe, frequently associated with the advection of colder air masses as can be seen from the corresponding θ_e anomaly at 850 hPa (Figure 8b). In addition, large-scale subsidence takes place over large parts of Europe (not shown). The resulting convection-inhibiting conditions primarily affect some areas in the central Alps, where TDs are found to be largely reduced.

In contrast for EA_+, the pattern is almost reversed with a southwesterly upper-level flow (Figure 8c). In many cases, this configuration results in the advection of subtropical, unstable air masses by low-pressure systems typically located ahead of the upper-level troughs, which also manifests in a
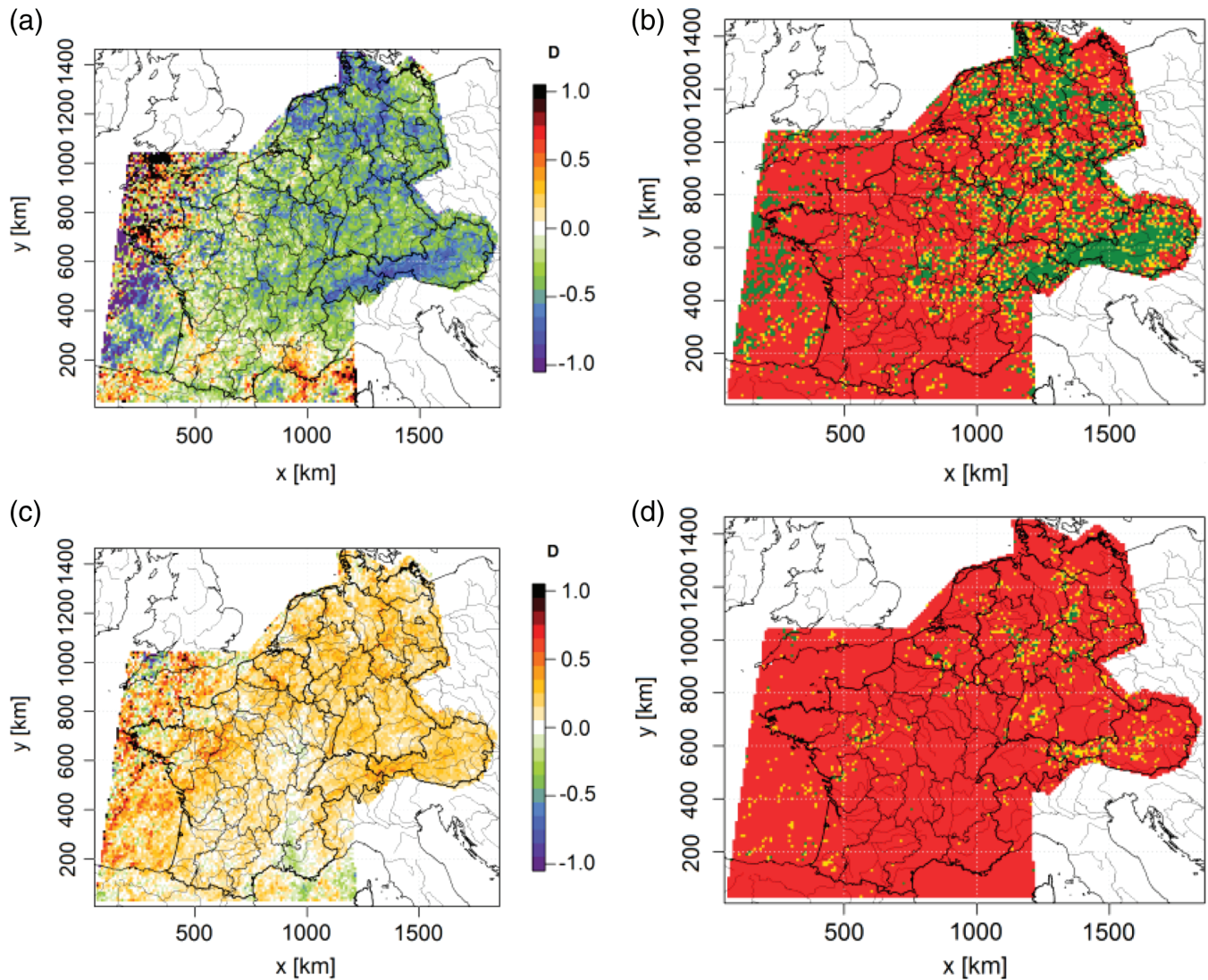
FIGURE 6 Relative deviation (D) of the monthly number of thunderstorm days (TDs) according to lightning data for the summer half-years between 2001 and 2014, quantified for months with (a) EA index < -0.5 (EA$_-$) and (c) EA index $> +0.5$ (EA$_+$) with respect to all months. (b) and (d) show the results of a two-sided bootstrap test with the level of significance $Si = 95\%$ (green), $Si = 90\%$ (yellow) and $Si < 90\%$ (red)

positive θ_e anomaly (Figure 8d). Convection initiation is facilitated by large-scale lifting connected to quasi-geostrophic forcing and, in some cases, by the ascending branch of the frontal secondary circulation. Together, these factors explain a substantial part of the widespread increase in both TDs and WMILX days during EA$_+$.

4.3.3 | Scandinavian pattern

Similar to the results for EA, the SCAND index also shows a certain influence on convective activity. During negative phases (SCAND$_-$ < -1; Figure 9a,b), the relative TD changes are rather weak, statistically significant only at a few grid points (approximately at 2%), and with a large spatial variability of the signals, which does not allow for a meaningful interpretation of the results. In contrast to the negative phase, the signal during SCAND$_+$ is spatially much more homogeneous

with a pronounced increase in TDs over Germany, reaching the highest values of all NHTPs for D (Figure 9c,d). Statistical significance increases to approximately 11% of all grid points (Germany north of $y = 800$ km). In addition, thunderstorm activity is also increased over Austria, Switzerland, northern Italy, and the Rhône estuary in southern France.

The relationship between SCAND and the frequency of WMILX days (Figure 10) confirms the above findings, but shows a much more homogeneous spatial distribution. The sign and magnitude of the relative deviations D are similar in almost all sub-regions for the respective SCAND pattern; only a few sub-regions in the southwest (northern Spain) show a reverse behaviour. During SCAND$_-$, the number of WMILX days is reduced by about half over the eastern and central parts of the investigation area. D is lowest over the North Sea and west of the English Channel (Figure 10a,b). Note, however, that convective activity according to the CWT
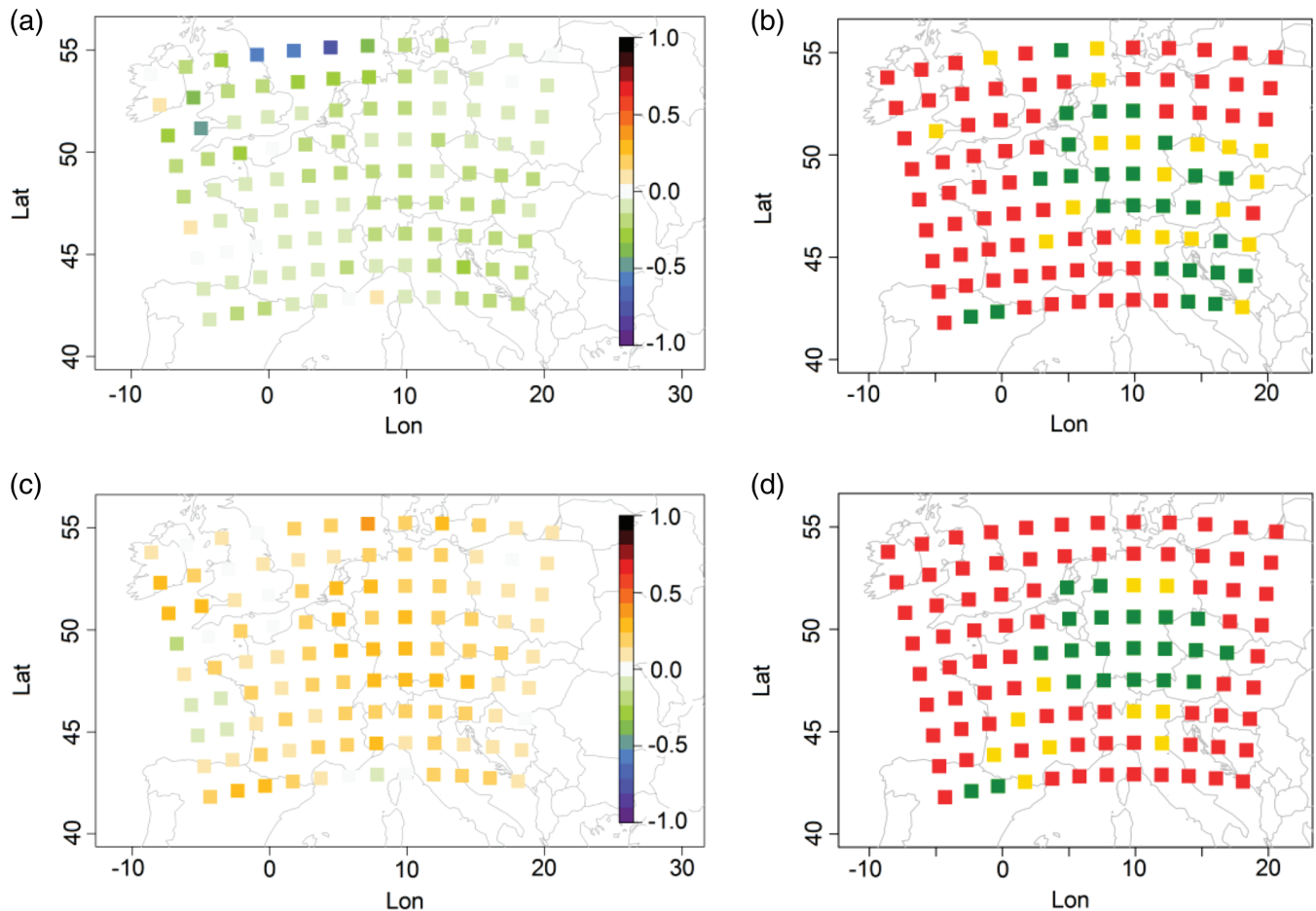
FIGURE 7 Relative deviation (D) of the monthly number of WMILX days according to the CWT classification for the summer half-years between 1982 and 2014 prevailing in the various sub-regions, quantified for months with (a) EA index < -0.5 (EA$_-$) and (c) EA index $> +0.5$ (EA$_+$) with respect to all months. (b) and (d) show the results of a two-sided bootstrap test with the level of significance $Si = 95\%$ (green), $Si = 90\%$ (yellow) and $Si < 90\%$ (red)

proxy is very low in that area (cf. Figure 4). For 47% of the sub-regions, the deviations are significant ($Si \geq 90\%$). During SCAND$_+$, WMILX days increase significantly over Germany with the highest values of D in the northwest (Figure 10c,d), analogously to the spatial distribution of TDs. The area of significant positive values extends far to the east and southeast to Slovakia and Hungary. The absolute maximum of D occurs over the North Sea and west of the English Channel, where WMILX frequency indeed doubles compared to the mean, but where convective activity is lowest as alluded to above. Overall, D is significant for half of the sub-regions.

The large-scale flow patterns associated with the two SCAND phases show a strong anomaly of the vectorial flow field and the zonal wind component at 300 hPa in a stripe between Ireland and the Baltic region (Figure 11a,c). During SCAND$_-$, the jet stream stretches across central Europe in a southeasterly direction (Figure 11a), inducing a northwesterly flow over the eastern parts of central Europe, characterized by cooler, stably stratified air masses advected from the north. This configuration is associated with a positive anomaly of

θ_e in the west and southwest, and a negative anomaly in the northwest, where the flow is strongest (Figure 11b). The decrease in both the number of TDs and WMILX days over the mentioned marine areas can be explained by a lack of large-scale lifting under the ridge, which is required for convection initiation over the usually stabilizing, cool sea water surrounding northern Europe.

In contrast during SCAND$_+$, the 300 hPa flow anomaly shows that this phase is characterized by strong ridges extending into northern Europe (Figure 11c). Eastern central Europe is located below the core region of the ridge (not shown), with favourable thermodynamic conditions. Over western Europe, there is some indication of the potential for troughs to occur, leading to the advection of unstable air masses at low levels and providing large-scale lifting. This effect is strongest over southern Scandinavia and northern Germany, where the increase in θ_e is largest (Figure 11d). Similar conditions were observed by Mohr *et al.* (2019), who identified that Scandinavian blocking, which corresponds to SCAND$_+$ (Cassou, 2008), is frequently associated with an increased odds of thunderstorm occurrence due to convection-favouring conditions
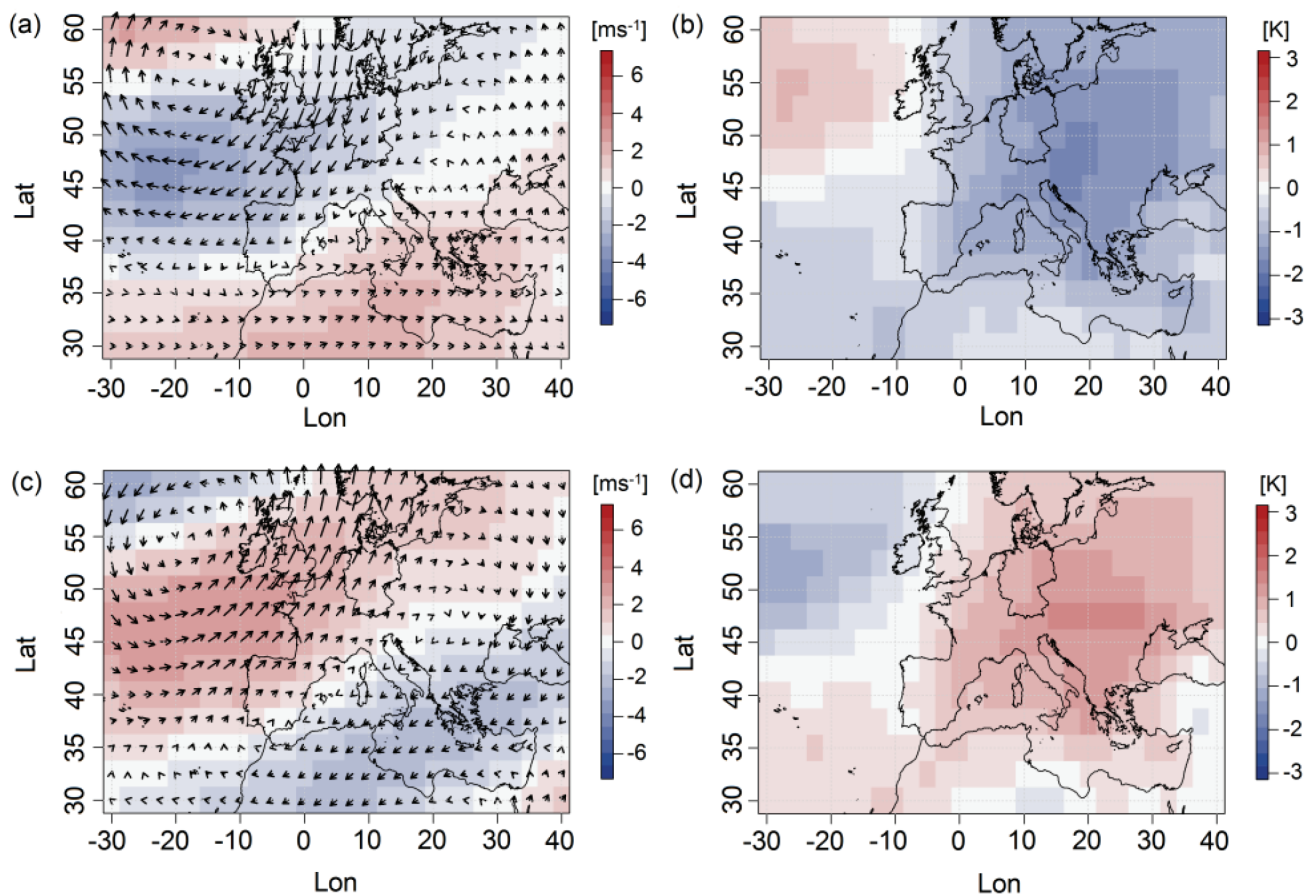
FIGURE 8 Average anomaly of (a) wind vectors and horizontal velocity [m/s] at 300 hPa, and (b) equivalent potential temperature θ_e [K] at 850 hPa during negative EA$_-$ phases. (c) and (d) are analogous for positive phases, EA$_+$

on its western flank (southwesterly advection of warm, moist and unstable air masses).

## 4.4 | Relation between sea-surface temperature and convective activity

Due to the high specific heat capacity of water compared to air and the large-scale meridional overturning circulation (MOC), the SST is characterized by a very low-frequency variability. Given the proximity of the Bay of Biscay to convective activity through central Europe, in the following we consider SST anomalies prevailing in that region (cf. section 2.4). Analogously to the teleconnection patterns, SST phases are defined based on the thresholds of 0.5 and -0.5 K limiting the positive (SST$_+$) and negative (SST$_-$) phases, respectively.

The results of the relation between SST and TDs exhibit a large spatial variability. During SST$_-$, mainly the eastern parts of the investigation area, in particular northern Germany, Austria, and northern Italy, experience a significant increase in TDs (not shown). In contrast over large parts of western and southern France, thunderstorm frequency increases during SST$_+$ (mostly significant; not shown).

Analogously to EA and SCAND, the sign of the relative deviations D during WMILX days is almost the same

in all sub-regions (Figure 12). For SST$_-$, strong decreases in the WMILX frequency are observed over the western sub-regions, which continually weaken in the eastward direction. Only a few sub-regions on the eastern fringe turn into weak positive anomalies. The WMILX anomaly during SST$_+$ is qualitatively similarly distributed, albeit with reversed signs, but similar levels of significance (57.4% of all sub-regions show relative deviations with $Si \geq 90\%$; Figure 12c,d). The number of WMILX days increases strongest over France with a maximum in the southwest.

Considering the large-scale anomalies of environmental conditions that coincide with SST anomalies, a strong relation both to 300 hPa geopotential and to θ_e is obvious. During SST$_-$ (Figure 13a), a pronounced cyclonic jet stream anomaly is present with its centre over northern France/southeastern England, causing invigorated flow over entire Europe. Along the French west coast, the northwesterly upper-level flow may additionally lead to the advection of cool and stably stratified air masses. The flow configuration during positive SST$_+$ (Figure 13c) is almost the reverse to SST$_-$ with a positive geopotential anomaly over the southern North Sea associated with a weaker flow at 300 hPa. As a result, preference is given to configurations with France to be located under the ridge and southwesterly flow at the Bay of Biscay. This
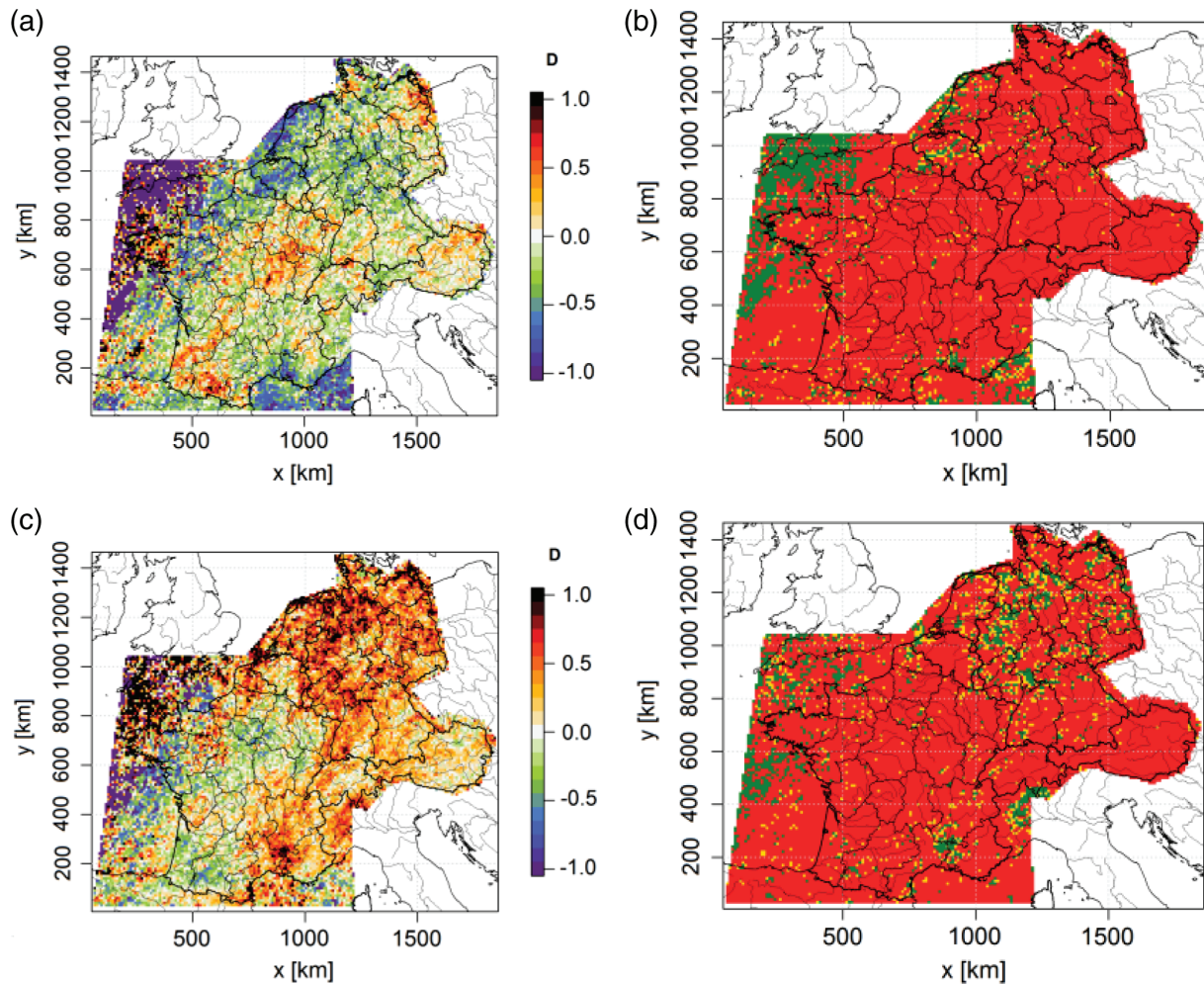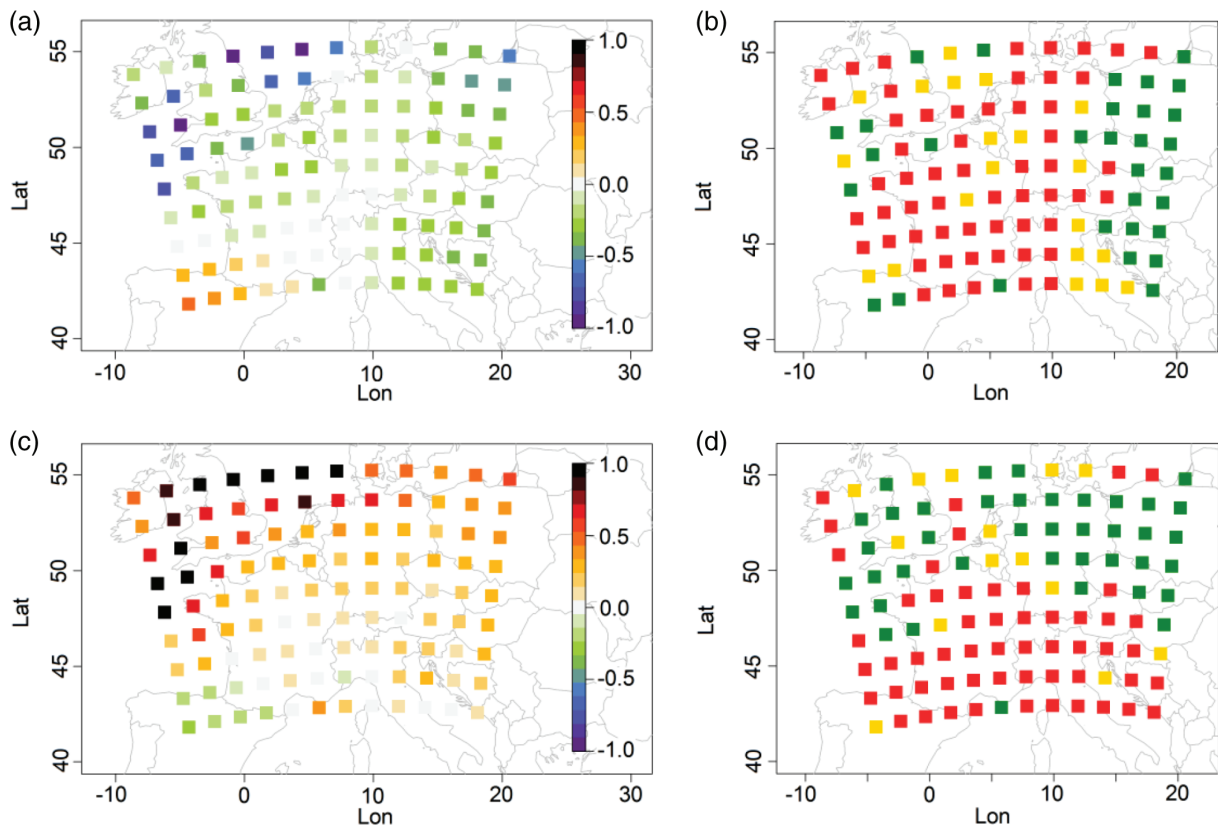
FIGURE 9 Same as Figure 6, but for (a,b) SCAND < -1.0 (SCAND$_-$) and (c,d) SCAND $> +1.0$ (SCAND$_+$)

situation often implies southerly advection of moist and warm air at low levels with sensible-heat fluxes towards the surface water accounting for the positive SST anomaly. Associated southerly flow aloft also has an increased likelihood for the advection of an elevated mixed layer (EML), known as the Spanish Plume over western France, which produces a conditionally unstable environment favourable to the development of severe convective storms (Carlson and Ludlam, 1968; Carlson *et al.*, 1983; Lanicci and Warner, 1991; Lewis and Gray, 2010; Kunz *et al.*, 2018). Overall, the influence of the SST anomalies is spatially extended and affects most parts of France and Spain in the case of SST$_-$, and entire western and central Europe in the case of SST$_+$. This finding suggests that the increase/decrease of WMILX days as discussed above is mainly thermodynamically driven by θ_e anomalies related to SST.

The anomaly pattern of the jet stream during SST$_-$ (Figure 13a) implies frequent troughs over the western regions, and goes along with convection-inhibiting conditions there. Although this effect becomes less significant farther to the east, a positive anomaly in the number of WMILX days would require a more frequent superposition of thermodynamically and dynamically favourable conditions for convection in this area. In this context, the increase in TDs in northern Germany (not shown) indicates that the pre-convective environment indeed becomes more favourable during SST$_-$, but this effect is not strong enough to exceed the thresholds of the meteorological parameters (cf. Table 3) required for the class WMILX to occur more frequently. Recall that, by approximation, WMILX is sufficient but not necessary for widespread convective activity.

Conversely, the anomaly pattern of the jet stream during SST$_+$ (Figure 13c) implies that southwestern France is often located upstream of a ridge, where convection-favouring conditions are mostly present both from a thermodynamic and dynamic point of view. Towards the east, the anomaly of WMILX days decreases, because large-scale dynamic lifting occurs less frequently there. Thus, there is a strong relationship between SST over the Bay of Biscay and convective activity across large parts of Europe. For the sub-regions located to the southwest, for example, the rank correlation coefficient according to Spearman between the time series of annual SST anomalies and the number of WMILX days is $r = .52$ ($Si \geq 95\%$).
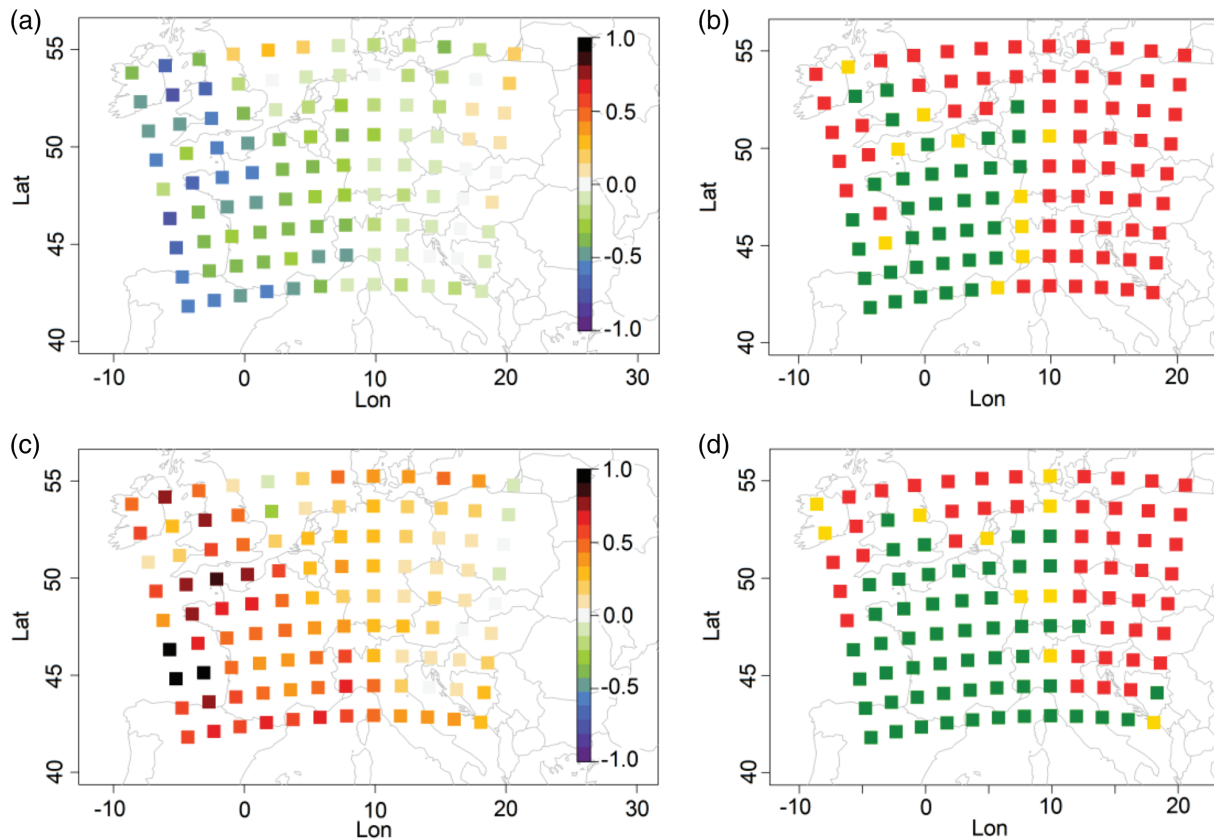
FIGURE 10 Same as Figure 7, but for (a,b) SCAND < −1.0 (SCAND₋) and (c,d) SCAND > +1.0 (SCAND₊)
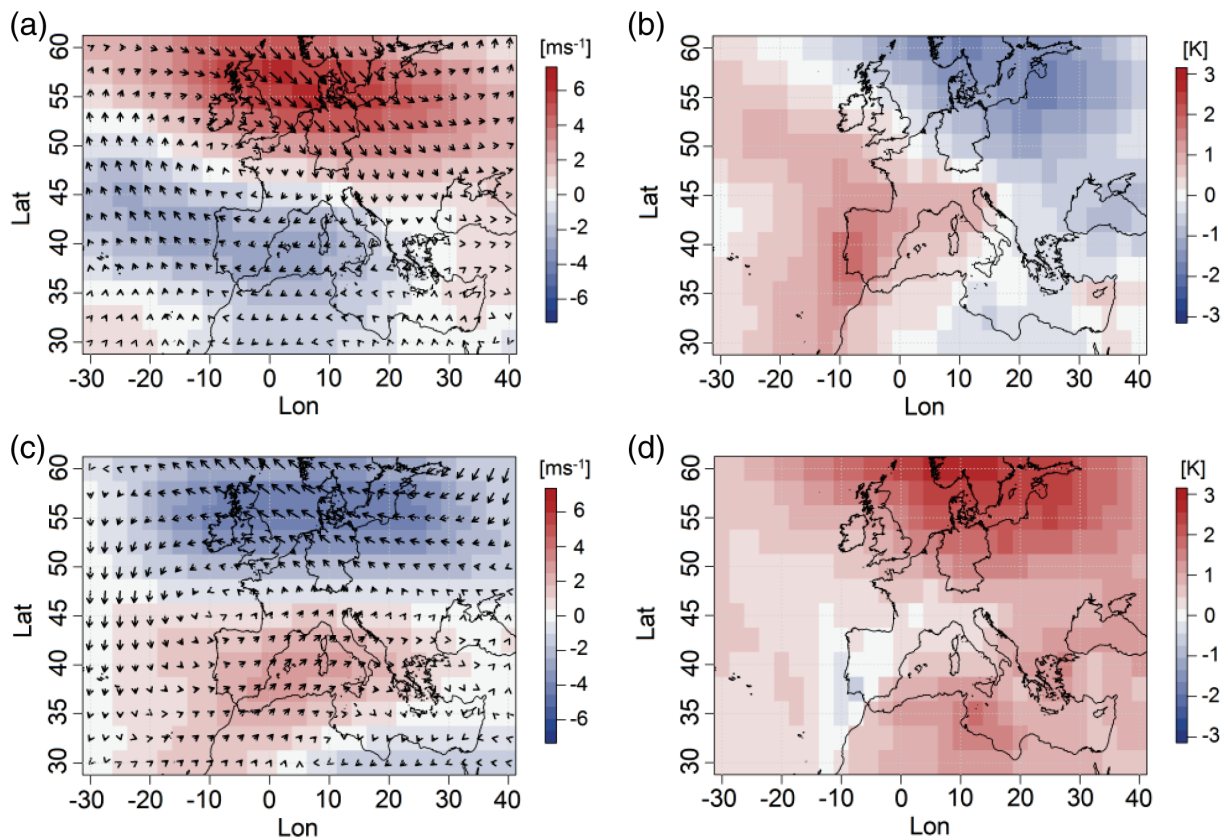
FIGURE 11 Same as Figure 8, but for (a,b) SCAND < −1.0 (SCAND₋) and (c,d) SCAND > +1.0 (SCAND₊)

FIGURE 12   Same as Figure 7, but for (a,b) SST anomaly < −0.5 K (SST$_-$) and (c,d) SST anomaly > +0.5 K (SST$_+$)

5 | DISCUSSION AND CONCLUSIONS

The large-scale driving mechanisms of thunderstorm activity have been investigated within a study domain comprising large parts of central and western Europe based on 14 years of lightning observations and 57 years of reanalysis data (April–September). For this purpose, a new multivariate proxy describing convective conditions of the atmosphere was developed separating those days from the continuum of possible atmospheric states that exhibit a high probability for widespread thunderstorm occurrence (sufficient condition). Based on the four variables equivalent-potential temperature (θ_e), precipitable water (pw), Surface Lifted Index (SLI), and vertical velocity (w), each day was classified as convection-favouring, neutral or convection-inhibiting, using objectively determined thresholds. The highest number of annual convection-favouring weather patterns occurred in a curved region extending from southern France to the eastern boundary of the study area. Characteristic convection-favouring flow patterns were obtained by applying a T-mode principal component analysis to the sample of 500 hPa geopotential fields (1200 UTC) defined by the convection-favouring days. Evaluating the proxy with respect to different reference areas allowed for spatially comparing the characteristic patterns. The relation between the long-term

variability of convective activity and natural climate variability was assessed investigating the impact of different atmospheric teleconnections and SST on environmental proxies.

Across the domain, convection-favouring conditions primarily occur ahead of upper-level troughs, consistent with similar studies (Kapsch *et al.*, 2012; Merino *et al.*, 2014; Punge and Kunz, 2016; Westermayer *et al.*, 2017; Mohr *et al.*, 2019; Taszarek *et al.*, 2019). In some regions, however, further flow configurations were shown to provide favourable pre-convective environments such as, for example, a broad upper-level low over the Adriatic Sea favouring thunderstorm occurrence in southern Poland. These results suggest that the convective environment is decisively influenced by the state of mid-tropospheric flow steering the large-scale thermodynamic and dynamic conditions relevant for convection. Simultaneously, favourable flow patterns often induce the advection of warm and moist air masses with two advection pathways prevailing: from southwesterly, subtropical regions via Spain and France, possibly in combination with an elevated mixed layer (Carlson and Ludlam, 1968; Carlson *et al.*, 1983; Lanicci and Warner, 1991) associated with a Spanish plume event (Morris, 1986; van Delden, 2001; Lewis and Gray, 2010), or from the Black Sea region via Poland and the northeastern parts of Germany.

Our research suggests that convection-favouring environments are highly impacted by large-scale mechanisms such
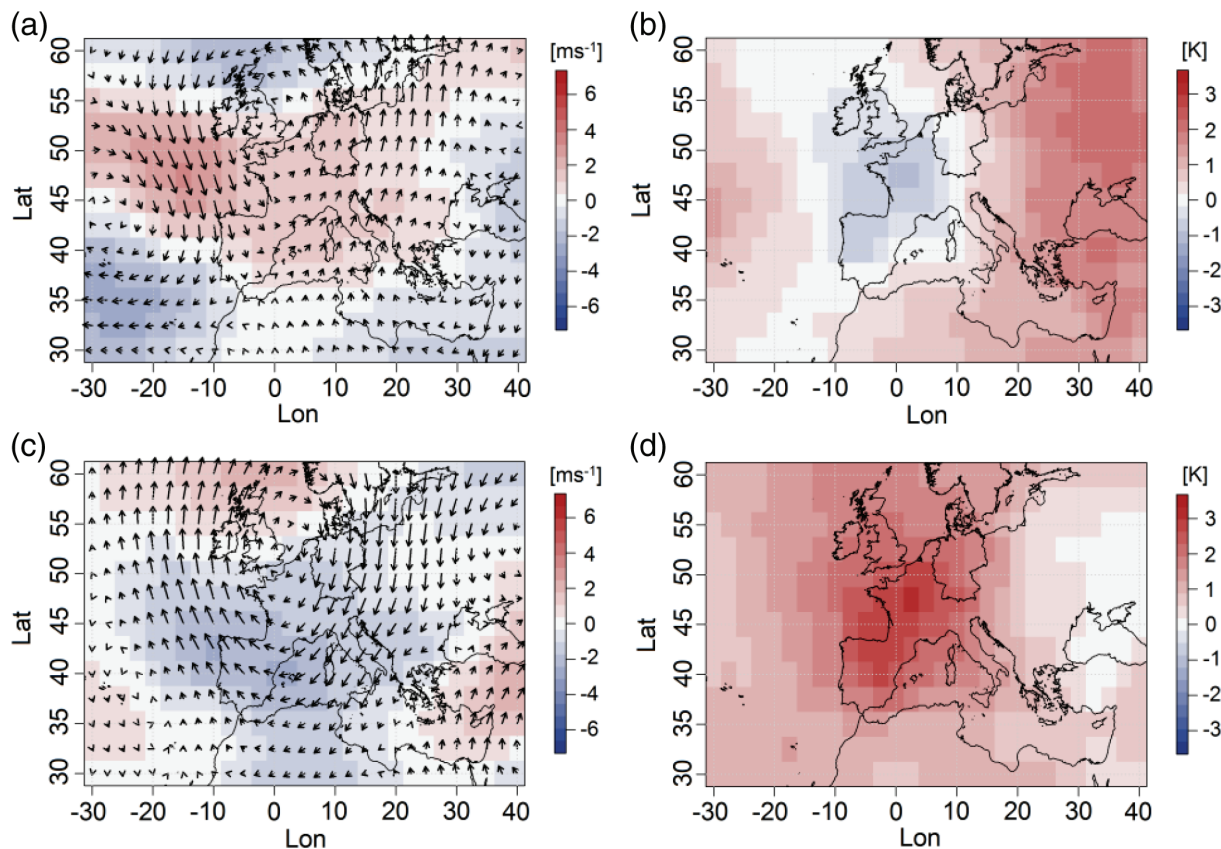
FIGURE 13 Same as Figure 8, but for (a,b) SST anomaly < −0.5 K (SST_−) and (c,d) SST anomaly > +0.5 K (SST_+)

as teleconnection patterns (NAO, EA and SCAND) and SST. The positive EA_+ phase, for example, is associated with more frequent troughs over western Europe, leading to a south-westerly upper-level flow over central Europe and, hence, an increased convection-favouring environment. During the positive SCAND_+ phase, a strong positive geopotential anomaly over northern Germany/southern Scandinavia together with a negative anomaly over western Europe favours convective activity primarily in northern Germany (cf. Mohr *et al.*, 2019). A particularly strong impact can be generally observed in regions where thunderstorm formation is comparatively rare, or requires very favourable pre-convective environments, such as coastal regions or marine areas. The combination of the results based on lightning data and the environmental proxy including large-scale forcing factors demonstrate and confirm the qualitatively consistent and robust role in teleconnection patterns, with the strongest signal from the EA pattern, in modulating convective activity. The analysis of the teleconnection patterns reveals that the geopotential field as a determining element of the large-scale atmospheric state is significantly linked to thunderstorm activity in central Europe. From a local influence perspective, clearer connections were obtained with respect to SST anomalies in the Bay of Biscay. In particular, the SST anomalies reveal their role as a significant factor of natural climate variability, modulating thermodynamic instability, and hence convective activity

(Molina *et al.*, 2016; Piazza *et al.*, 2016; Wills *et al.*, 2016; Miglietta *et al.*, 2017).

An advantage of the approach used herein is that the newly developed multivariate proxy of convective weather types allowed analysis of convective activity based on a long-term series of high-resolution reanalysis data, leading to statistically more significant results as compared to short-duration observational datasets used in earlier work (Giaiotti *et al.*, 2003). By linking these favourable convective conditions to both flow patterns and teleconnection indices, we were able to investigate the crucial role of the geopotential field on a wide range of temporal scales. A potential weakness of the research methodology, however, is that the procedure mapping the continuum of possible states of the geopotential field on a discrete set of characteristic patterns does not yield unambiguous results. Slightly different patterns might have been obtained using alternative approaches such as K-means clustering. However, the analysis of maximum loadings confirms that the rotated PCs presented in this article do indeed represent the actual flow patterns reasonably well. It is also likely that the convection-favouring weather type (WMILX) used here is not necessarily representative of convective frequency where topographic forcing and instability are the dominant drivers of thunderstorm occurrence. This applies, for example, to the noted deficiency in the mapping of the convective environment over northern Italy and other mountainous regions.

However, this deficiency is at least partly due to the reanalysis data not sufficiently resolving orographically induced circulations and resulting convergence zones relevant for triggering convection. It can also explain part of the inconsistency between our conclusions of the limited impact for the NAO and other studies that considered shorter observed time series or a time shift between convective events and NAO (Giaiotti *et al.*, 2003). However, it should also be noted that in terms of precipitation, NAO only explains some 22% of summertime variability in mean-sea-level pressure (Folland *et al.*, 2009) and a similar fraction of precipitation variability (Zveryaev and Allan, 2010), and thus our results may simply suggest that other teleconnection signals modulate convective frequency more prominently. Another potential weakness of our research is that we did not split the observation period into a training and a verification period. Because of the short time period of 14 years, when data were available in our archives, we decided to rely on one dataset only.

Teleconnections between atmospheric phenomena and climate signals are complex interactions that are extremely challenging to consider in isolation, as noted in the recent review by Stan *et al.* (2017). It is important to note that while analysis of teleconnections can reveal important information about the processes driving the variability of convective weather (e.g. Elsner and Widen, 2013; Elsner *et al.*, 2016; Gensini and Marinaro, 2016; Molina *et al.*, 2018) or other atmospheric phenomena (Gastineau and Frankignoul, 2015), these signals are not independent of each other, but often interlinked. For example, research exploring the monthly variability of precipitation over Europe identified a significant contribution from evaporation over land (Zveryaev and Allan, 2010), which could imply preconditioning in terms of both soil moisture and periods of drought. The significant impact of the atmospheric teleconnections identified herein, together with the role of SST variability on convective activity in Europe, similar to recently noted interactions (Piazza *et al.*, 2016; Wills *et al.*, 2016), motivates further analysis to explore both the joint variability along with other drivers of atmospheric–oceanic variability over the region that may be more remote, such as El Niño/Southern Oscillation (ENSO: cf. Lee *et al.*, 2013; Allen *et al.*, 2015b; Cook *et al.*, 2017; Molina *et al.*, 2018). This is particularly necessary to identify residual variance of annual convective activity to further investigate crucial influencing factors, which are still unknown.

ORCID

Michael Kunz https://orcid.org/0000-0002-0202-9558
John T. Allen https://orcid.org/0000-0002-2036-0666
Susanna Mohr https://orcid.org/0000-0002-3556-7299

REFERENCES

Allen, J.T. and Karoly, D.J. (2014) A climatology of Australian severe thunderstorm environments 1979–2011: inter-annual variability and ENSO influence. *International Journal of Climatology*, 34, 81–97.

Allen, J.T., Tippett, M.K. and Sobel, A.H. (2015a) An empirical model relating US monthly hail occurrence to large-scale meteorological environment. *Journal of Advances in Modeling Earth Systems*, 7, 226–243.

Allen, J.T., Tippett, M.K. and Sobel, A.H. (2015b) Influence of the El Niño/Southern Oscillation on tornado and hail frequency in the United States. *Nature Geoscience*, 8, 278–283.

Allen, J.T., Molina, M.J. and Gensini, V.A. (2018) Modulation of annual cycle of tornadoes by El Niño–Southern Oscillation. *Geophysical Research Letters*, 45, 5708–5717.

Anderson, G. and Klugmann, D. (2014) A European lightning density analysis using 5 years of ATDnet data. *Natural Hazards and Earth System Sciences*, 14, 815–829.

Baggett, C.F., Nardi, K.M., Childs, S.J., Zito, S.N., Barnes, E.A. and Maloney, E.D. (2018) Skillful subseasonal forecasts of weekly tornado and hail activity using the Madden–Julian Oscillation. *Journal of Geophysical Research – Atmospheres*, 123(22), 12661–12675.

Barnston, A.G. and Livezey, R.E. (1987) Classification, seasonality and persistence of low-frequency atmospheric circulation patterns. *Monthly Weather Review*, 115, 1083–1126.

Barrett, B.S. and Gensini, V.A. (2013) Variability of central United States April–May tornado day likelihood by phase of the Madden–Julian Oscillation. *Geophysical Research Letters*, 40, 2790–2795.

Bissolli, P. and Dittmann, E. (2001) The objective weather types classification of the German Weather Service and its possibilities of application to environmental and meteorological investigations. *Meteorologische Zeitschrift*, 10, 253–260.

Bissolli, P., Grieser, J., Dotzek, N. and Welsch, M. (2007) Tornadoes in Germany 1950–2003 and their relation to particular weather conditions. *Global and Planetary Change*, 57, 124–138.

Blamey, R.C., Middleton, C., Lennard, C. and Reason, C.J.C. (2017) A climatology of potential severe convective environments across South Africa. *Climate Dynamics*, 49, 2161–2178.

Brooks, H.E. (2009) Proximity soundings for severe convection for Europe and the United States from reanalysis data. *Atmospheric Research*, 93, 546–553.

Brooks, H.E., Lee, J.W. and Craven, J.P. (2003) The spatial distribution of severe thunderstorm and tornado environments from global reanalysis data. *Atmospheric Research*, 67, 73–94.

Bueh, C. and Nakamura, H. (2007) Scandinavian pattern and its climatic impact. *Quarterly Journal of Royal Meteorological Society*, 133, 2117–2131.

Carlson, T.N. and Ludlam, F.H. (1968) Conditions for the occurrence of severe local storms. *Tellus*, 20, 203–226.

Carlson, T.N., Benjamin, S.G., Forbes, G.S. and Li, Y.F. (1983) Elevated mixed layers in the regional severe storm environment: conceptual model and case studies. *Monthly Weather Review*, 111, 1453–1474.

Casanueva Vicente, A., Rodríguez Puebla, C., Frías Domínguez, M.D. and González Reviriego, N. (2014) Variability of extreme precipitation over Europe and its relationships with teleconnection patterns. *Hydrology and Earth System Sciences*, 18, 709–725.

Cassou, C. (2008) Intraseasonal interaction between the Madden–Julian Oscillation and the North Atlantic Oscillation. *Nature*, 455, 523–527.

Cook, A.R., Leslie, L.M., Parsons, D.B. and Schaefer, J.T. (2017) The impact of El Niño–Southern Oscillation (ENSO) on winter and early spring US tornado outbreaks. *Journal of Applied Meteorology and Climatology*, 56, 2455–2478.

van Delden, A. (2001) The synoptic setting of thunderstorms in western Europe. *Atmospheric Research*, 56, 89–110.

Dowdy, A.J. (2016) Seasonal forecasting of lightning and thunderstorm activity in tropical and temperate regions of the world. *Scientific Reports*, 6, 20874.

Elsner, J.B. and Widen, H.M. (2013) Predicting spring tornado activity in the central Great Plains by 1 March. *Monthly Weather Review*, 142, 259–267.

Elsner, J.B., Jagger, T.H. and Fricker, T. (2016) Statistical models for tornado climatology: long and short-term views. *PLoS One*, 11(e0166), 895.

Feser, F., Rockel, B., von Storch, H., Winterfeldt, J. and Zahn, M. (2011) Regional climate models add value to global model data: a review and selected examples. *Bulletin of the American Meteorological Society*, 92, 1181–1192.

Feudale, L. and Manzato, A. (2014) Cloud-to-ground lightning distribution and its relationship with orography and anthropogenic emissions in the Po Valley. *Journal of Applied Meteorology and Climatology*, 53, 2651–2670.

Folland, C.K., Knight, J., Linderholm, H.W., Fereday, D., Ineson, S. and Hurrell, J.W. (2009) The summer North Atlantic Oscillation: past, present, and future. *Journal of Climate*, 22, 1082–1103.

Galway, J.G. (1956) The lifted index as a predictor of latent instability. *Bulletin of the American Meteorological Society*, 37, 528–529.

Gastineau, G. and Frankignoul, C. (2015) Influence of the North Atlantic SST variability on the atmospheric circulation during the twentieth century. *Journal of Climate*, 28, 1396–1416.

Gensini, V.A. and Allen, J.T. (2018) US hail frequency and the global wind oscillation. *Geophysical Research Letters*, 45, 1611–1620.

Gensini, V.A. and Marinaro, A. (2016) Tornado frequency in the United States related to global relative angular momentum. *Monthly Weather Review*, 144, 801–810.

Gensini, V.A. and Mote, T.L. (2014) Estimations of hazardous convective weather in the United States using dynamical downscaling. *Journal of Climate*, 27, 6581–6589.

Geyer, B. (2014) High-resolution atmospheric reconstruction for Europe 1948–2012: coastDat2. *Earth System Science Data*, 6, 147–164.

Giaiotti, D., Nordio, S. and Stel, F. (2003) The climatology of hail in the plain of Friuli Venezia Giulia. *Atmospheric Research*, 67, 247–259.

Groenemeijer, P., Púčik, T., Holzer, A.M., Antonescu, B., Riemann-Campe, K., Schultz, D.M., Kühne, T., Feuerstein, B., Brooks, H.E., Doswell, C.A., III, Koppert, H.J. and Sausen, R. (2017) Severe convective storms in Europe: ten years of research and education at the European Severe Storms Laboratory. *Bulletin of the American Meteorological Society*, 98, 2641–2651.

Guimares Nobre, G., Jongman, B., Aerts, J. and Ward, P.J. (2017) The role of climate variability in extreme floods in Europe. *Environmental Research Letters*, 12, 084012.

Heidke, P. (1926) Berechnung des Erfolges und der Güte der Windstärkenvorhersagen im Sturmwarnungsdienst. *Geografiska Annaler*, 8, 301–349.

Hoogewind, K.A., Baldwin, M.E. and Trapp, R.J. (2017) The impact of climate change on hazardous convective weather in the United States: insight from high-resolution dynamical downscaling. *Journal of Climate*, 30, 10081–10100.

Hurrell, J.W., Kushnir, Y., Ottersen, G. and Visbeck, M. (2003) The North Atlantic Oscillation: climate significance and environmental impact. *Geophysical Monograph*, 134. American Geophysical Union, 279.

Huth, R. (1996) Properties of the circulation classification scheme based on the rotated principal component analysis. *Meteorology and Atmospheric Physics*, 59, 217–233.

Huth, R. (2000) A circulation classification scheme applicable in GCM studies. *Theoretical and Applied Climatology*, 67, 1–18.

Kalnay, E., Kanamitsu, M., Kistler, R., Collins, W., Deaven, D., Gandin, L., Iredell, M., Saha, S., White, G., Woollen, J., Zhu, Y., Leetmaa, A., Reynolds, F., Chelliah, M., Ebisuzaki, W., Higgins, W., Janowiak, J., Mo, K., Ropelewski, C., Wang, J., Jenne, F. and Joseph, D. (1996) The NCEP/NCAR 40-year reanalysis project. *Bulletin of the American Meteorological Society*, 77, 437–472.

Kanamitsu, M., Ebisuzaki, W., Woollen, J., Yang, S.K., Hnilo, J.J., Fiorino, M. and Potter, G.L. (2002) NCEP–DOE AMIP-II Reanalysis (R-2). *Bulletin of the American Meteorological Society*, 83, 1631–1644.

Kapsch, M.-L., Kunz, M., Vitolo, R. and Economou, T. (2012) Long-term trends of hail-related weather types in an ensemble of regional climate models using a Bayesian approach. *Journal of Geophysical Research*, 117(D15), 107. https://doi.org/10.1029/2011JD0185.

Kendon, E.J., Ban, N., Roberts, N.M., Fowler, H.J., Roberts, M.J., Chan, S.C., Evans, J.P., Fosser, G. and Wilkinson, J.M. (2017) Do convection-permitting regional climate models improve projections of future precipitation change? *Bulletin of the American Meteorological Society*, 98, 79–93.

Krichak, S.O. and Alpert, P. (2005) Decadal trends in the east Atlantic–west Russia pattern and Mediterranean precipitation. *International Journal of Climatology*, 25, 183–192.

Kunz, M., Sander, J. and Kottmeier, C. (2009) Recent trends of thunderstorm and hailstorm frequency and their relation to atmospheric characteristics in southwest Germany. *International Journal of Climatology*, 29, 2283–2297.

Kunz, M., Blahak, U., Handwerker, J., Schmidberger, M., Punge, H.J., Mohr, S., Fluck, E. and Bedka, K.M. (2018) The severe hailstorm in southwest Germany on 28 July 2013: characteristics, impacts and meteorological conditions. *Quarterly Journal of the Royal Meteorological Society*, 144(710), 231–250.

Lanicci, J.M. and Warner, T.T. (1991) A synoptic climatology of the elevated mixed-layer inversion over the southern Great Plains in spring.

Part I: Structure, dynamics, and seasonal evolution. *Weather and Forecasting*, 6, 181–197.

Lee, S.K., Atlas, R., Enfield, D., Wang, C. and Liu, H. (2013) Is there an optimal ENSO pattern that enhances large-scale atmospheric processes conducive to tornado outbreaks in the United States? *Journal of Climate*, 26, 1626–1642.

Lewis, M.W. and Gray, S.L. (2010) Categorisation of synoptic environments associated with mesoscale convective systems over the UK. *Atmospheric Research*, 97, 194–213.

Madonna, E., Ginsbourger, D. and Martius, O. (2018) A Poisson regression approach to model monthly hail occurrence in northern Switzerland using large-scale environmental variables. *Atmospheric Research*, 203, 261–274.

Martius, O., Hering, A., Kunz, M., Manzato, A., Mohr, S., Nisi, L. and Trefald, S. (2018) Challenges and recent advances in hail research. *Bulletin of the American Meteorological Society*, 99, ES51–ES54.

Marzban, C. and Schaefer, J.T. (2001) The correlation between US tornadoes and Pacific sea surface temperatures. *Monthly Weather Review*, 129, 884–895.

Merino, A., Wu, X., Gascón, E., Berthet, C., García-Ortega, E. and Dessens, J. (2014) Hailstorms in southwestern France: incidence and atmospheric characterization. *Atmospheric Research*, 140–141, 61–75.

Miglietta, M.M., Mazon, J., Motola, V. and Pasini, A. (2017) Effect of a positive sea surface temperature anomaly on a Mediterranean tornadic supercell. *Scientific Reports*, 7, 12828.

Mohr, S. and Kunz, M. (2013) Recent trends and variabilities of convective parameters relevant for hail events in Germany and Europe. *Atmospheric Research*, 123, 211–228.

Mohr, S., Kunz, M. and Geyer, B. (2015a) Hail potential in Europe based on a regional climate model hindcast. *Geophysical Research Letters*, 42, 10904–10912.

Mohr, S., Kunz, M. and Keuler, K. (2015b) Development and application of a logistic model to estimate the past and future hail potential in Germany. *Journal of Geophysical Research: Atmospheres*, 120, 3939–3956.

Mohr, S., Wandel, J., Lenggenhager, S. and Martius, O. (2019) Relationship between atmospheric blocking and warm-season thunderstorms over western and central Europe. *Quarterly Journal of Royal Meteorological Society*, 1–17. https://doi.org/10.1002/qj.3603.

Molina, M.J., Timmer, R.P. and Allen, J.T. (2016) Importance of the Gulf of Mexico as a climate driver for US severe thunderstorm activity. *Geophysical Research Letters*, 43, 12295–12304.

Molina, M.J., Allen, J.T. and Gensini, V.A. (2018) The Gulf of Mexico and ENSO influence on subseasonal and seasonal CONUS winter tornado variability. *Journal of Applied Meteorology and Climatology*, 57, 2439–2463.

Morris, R.M. (1986) The Spanish plume – testing the forecaster's nerve. *Meteorological Magazine*, 115(1372), 349–357.

Murphy, A.H. (1973) A new vector partition of the probability score. *Journal of Applied Meteorology*, 12, 595–600.

Nisi, L., Martius, O., Hering, A., Kunz, M. and Germann, U. (2016) Spatial and temporal distribution of hailstorms in the Alpine region: a long-term, high resolution, radar-based analysis. *Quarterly Journal of Royal Meteorological Society*, 142, 1590–1604.

Nisi, L., Hering, A., Germann, U. and Martius, O. (2018) A 15-year hail streak climatology for the Alpine region. *Quarterly Journal of Royal Meteorological Society*, 144(714), 1429–1449.

North, G.R., Bell, T.L., Cahalan, R.F. and Moeng, F.J. (1982) Sampling errors in the estimation of empirical orthogonal functions. *Monthly Weather Review*, 110, 699–706.

O'Lenic, E.A. and Livezey, R.E. (1988) Practical considerations in the use of rotated principal component analysis (RPCA) in diagnostic studies of upper-air height fields. *Monthly Weather Review*, 116, 1682–1689.

Philipp, A. (2009) Comparison of principal component and cluster analysis for classifying circulation pattern sequences for the European domain. *Theoretical and Applied Climatology*, 96, 31–41.

Piazza, M., Terray, L., Boé, J., Maisonnave, E. and Sanchez-Gomez, E. (2016) Influence of small-scale North Atlantic sea surface temperature patterns on the marine boundary layer and free troposphere: a study using the atmospheric ARPEGE model. *Climate Dynamics*, 46, 1699–1717.

Pinto, O., Jr. (2015) Thunderstorm climatology of Brazil: ENSO and tropical Atlantic connections. *International Journal of Climatology*, 35, 871–878.

Piper DA. (2017) *Untersuchung der Gewitteraktivität und der relevanten großräumigen Steuerungsmechanismen über Mittel- und Westeuropa*. Wiss. Ber. Instit. Meteorol. Klimaf., No. 73, Karlsruhe Institute of Technology (KIT), KIT Scientific Publishing, Karlsruhe, Germany.

Piper, D.A. and Kunz, M. (2017) Spatiotemporal variability of lightning activity in Europe and the relation to the North Atlantic Oscillation teleconnection pattern. *Natural Hazards and Earth System Sciences*, 17, 1319–1336.

Pohjola, H. and Mäkelä, A. (2013) The comparison of GLD360 and EUCLID lightning location systems in Europe. *Atmospheric Research*, 123, 117–128.

Prein, A.F. and Holland, G.J. (2018) Global estimates of damaging hail hazard. *Weather and Climate Extremes*, 22, 10–23.

Punge, H.J. and Kunz, M. (2016) Hail observations and hailstorm characteristics in Europe: a review. *Atmospheric Research*, 176–177, 159–184.

Punge, H.J., Bedka, K.M., Kunz, M. and Reinbold, A. (2017) Hail frequency estimation across Europe based on a combination of overshooting top detections and the ERA-Interim reanalysis. *Atmospheric Research*, 198, 34–43.

Rädler, A.T., Groenemeijer, P., Faust, E. and Sausen, R. (2018) Detecting severe weather trends using an additive regressive convective hazard model (AR-CHaMo). *Journal of Applied Meteorology and Climatology*, 57, 569–587.

Rasmussen, K.L., Prein, A.F., Rasmussen, R.M., Ikeda, K. and Liu, C. (2017) Changes in the convective population and thermodynamic environments in convection-permitting regional climate simulations over the United States. *Climate Dynamics*, 1–26. https://doi.org/10.1007/s00382-017-4000-7.

Reynolds, R.W., Rayner, N.A., Smith, T.M., Stokes, D.C. and Wang, W. (2002) An improved *in situ* and satellite SST analysis for climate. *Journal of Climate*, 15, 1609–1625.

Richman, M.B. (1986) Rotation of principal components. *Journal of Climatology*, 6, 293–335.

Robinson, E.D., Trapp, R.J. and Baldwin, M.E. (2013) The geospatial and temporal distributions of severe thunderstorms from high-resolution dynamical downscaling. *Journal of Applied Meteorology and Climatology*, 52, 2147–2161.

Rockel, B., Will, A. and Hense, A. (2008) The regional climate model COSMO-CLM (CCLM). *Meteorologische Zeitschrift*, 17, 347–348.

Schiemann, R. and Frei, C. (2010) How to quantify the resolution of surface climate by circulation types: an example for Alpine precipitation. *Physics and Chemistry of the Earth*, 35, 403–410.

Schulz, W., Diendorfer, G., Pedeboy, S. and Poelman, D.R. (2016) The European lightning location system EUCLID. Part 1: Performance analysis and validation. *Natural Hazards and Earth System Sciences*, 16, 595–605.

Shaman, J. (2014) The seasonal effects of ENSO on European precipitation: observational analysis. *Journal of Climate*, 27, 6423–6438.

Stan, C., Straus, D.M., Frederiksen, J.S., Lin, H., Maloney, E.D. and Schumacher, C. (2017) Review of tropical–extratropical teleconnections on intraseasonal time scales. *Reviews of Geophysics*, 55, 902–937.

von Storch, H. and Zwiers, F.W. (2001) *Statistical Analysis in Climate Research*. Cambridge, UK: Cambridge University Press.

Taszarek, M., Allen, J., Púčik, T., Groenemeijer, P., Czernecki, B., Kolendowicz, L., Lagouvardos, K., Kotroni, V. and Schulz, W. (2019) A climatology of thunderstorms across Europe from a synthesis of multiple data sources. *Journal of Climate*, 32, 1813–1837.

Thompson, D.B. and Roundy, P.E. (2013) The relationship between the Madden–Julian oscillation and US violent tornado outbreaks in the spring. *Monthly Weather Review*, 141, 2087–2095.

Tippett, M.K. (2018) Robustness of relations between the MJO and US tornado occurrence. *Monthly Weather Review*, 146, 3873–3884.

Tippett, M.K., Allen, J.T., Gensini, V.A. and Brooks, H.E. (2015) Climate and hazardous convective weather. *Current Climate Change Reports*, 1, 60–73.

Trapp, R.J. and Hoogewind, K.A. (2018) Exploring a possible connection between US tornado activity and Arctic Sea ice. *npj Climate and Atmospheric Science*, 1, 14. https://doi.org/10.1038/s41612-018-0025-9.

Trapp, R.J., Robinson, E.D., Baldwin, M.E., Diffenbaugh, N.S. and Schwedler, B.R. (2011) Regional climate of hazardous convective weather through high-resolution dynamical downscaling. *Climate Dynamics*, 37, 677–688.

Wallace, J.M. and Gutzler, D.S. (1981) Teleconnections in the geopotential height field during the Northern Hemisphere winter. *Monthly Weather Review*, 109, 784–812.

Wapler, K. (2013) High-resolution climatology of lightning characteristics within central Europe. *Meteorology and Atmospheric Physics*, 122, 175–184.

Wapler, K. and James, P. (2015) Thunderstorm occurrence and characteristics in central Europe under different synoptic conditions. *Atmospheric Research*, 158, 231–244.

Westermayer, A.T., Groenemeijer, P., Pistotnik, G., Sausen, R. and Faust, E. (2017) Identification of favorable environments for thunderstorms in reanalysis data. *Meteorologische Zeitschrift*, 26, 59–70.

Wilks, D.S. (2011) *Statistical Methods in the Atmospheric Sciences*. San Diego, CA: Academic Press.

Wills, S.M., Thompson, D.W. and Ciasto, L.M. (2016) On the observed relationships between variability in Gulf Stream sea surface temperatures and the atmospheric circulation over the North Atlantic. *Journal of Climate*, 29, 3719–3730.

Zveryaev, I.I. and Allan, R.P. (2010) Summertime precipitation variability over Europe and its links to atmospheric dynamics and evaporation. *Journal of Geophysical Research*, 115(D12), 1–12. https://doi.org/10.1029/2008JD011213.

APPENDIX: SKILL SCORES

A.1. Heidke skill score

The Heidke Skill Score that Heidke (1926) used for categorical verification of rare events is defined as

$$HSS = \frac{2(a \cdot d - b \cdot c)}{(a+c)(c+d) + (a+b)(b+d)}, \qquad (A1)$$

where a represents the correct event forecasts, b the false alarms, c the misses, and d the non-events computed from a 2×2 contingency table (Wilks, 2011). The HSS accounts for both false alarms and positive events and can be interpreted as a percentage improvement over a reference forecast. The range is from $+1$ to -1, with the former for a perfect forecast; a value equal to zero implies random behaviour.

A.2. Brier Skill Score

The Brier Skill Score BSS is based on the Brier Score (BS) frequently used for the verification of probabilistic forecasts:

$$BSS = 1 - \frac{BS}{BS_{ref}}. \qquad (A2)$$

In its basic formulation, BS describes for a set of n predicted (binary) events the mean squared deviations of predicted occurrence probability y_k and actual occurrence o_k ($o_k \in \{0;1\}$):

$$BS = \frac{1}{n} \sum_{k=1}^{n} (y_k - o_k)^2. \qquad (A3)$$

For the evaluation of the CWTs, BS is transformed into a skill score with a range from -1 to 1, the latter for a perfect forecast (Schiemann and Frei, 2010). According to Murphy (1973), BS can be expressed as the sum of three terms

$$BS = \frac{1}{n} \sum_{t=1}^{T} N_t (y_t - \overline{o}_t)^2 - \frac{1}{n} \sum_{t=1}^{T} N_t (\overline{o}_t - \overline{o})^2 + \overline{o}(1 - \overline{o}), \quad (A4)$$

with the classes t $(1 \leq t \leq T)$ of the size N_t, y_t as the predicted probability, $\bar{o}_t = 1/N_t \sum_{k \in N_k} o_k$ as the relative probability of event in the t-th class, and $\bar{o} = 1/n \sum_{k=1}^{n} o_k = 1/n \sum_{t=1}^{T} N_t \bar{o}_t$ as the relative frequency related to all classes.

In Equation A4, the first term on the right-hand side is a measure of the reliability of the forecast, which is zero for the CWT proxy (the predicted probability y_t for the weather pattern t corresponds to the relative frequency $\bar{o}_t$). The second term is a measure of the resolution of the forecast and describes how often the event occurs in the t-th class compared to all weather patterns, yielding the skill of the

classification. The last term is a measure of the uncertainty inherent in the events, which does not depend on the class division (Murphy, 1973).

Substituting Equation A4 into A2 yields (Wilks, 2011):

$$BSS = \frac{\text{Resolution} - \text{Reliability}}{\text{Uncertainty}} = \frac{\sum_{t=1}^{T} N_t (y_t - \bar{o})^2}{\bar{o}(1 - \bar{o})}. \quad (A5)$$

This equation is used in this article to indicate the suitability of a specific CWT classification and to separate the two classes of convective day (*Yes/No*) as a scalar value.